Malaysian Journal of Analytical Sciences (MJAS)
Published by Malaysian Analytical Sciences Society

CHEMICAL SYNTHESIS OF METAL OXIDE NANOPARTICLES VIA IONIC LIQUID AS CAPPING AGENT: PRINCIPLE, PREPARATION AND APPLICATIONS

(Sintesis Kimia Logam Oksida Nanozarah Melalui Cecair Ionik Sebagai Ejen Pembekat: Prinsip, Penyediaan dan Aplikasi)

Nurul Syafiqah Tapak[1,2], Mohd Azizi Nawawi[2], Ahmad Husaini Mohamed[1], Eddie Tan Ti Tjih[3], Yusairie Mohd[2], Ahmad Hazri Bin Ab Rashid[4], Jaafar Abdullah[5*], Nor Azah Yusof [5], Nor Monica Ahmad[1,6*]

[1]School of Chemistry and Environment,
Faculty of Applied Sciences,
Universiti Teknologi MARA, Cawangan Negeri Sembilan, Kampus Kuala Pilah,
72000 Kuala Pilah, Malaysia
[2] School of Chemistry and Environment,
Faculty of Applied Sciences,
Universiti Teknologi MARA, 40450 Shah Alam, Malaysia
[3]School of Industrial Technology,
Faculty of Applied Sciences,
Universiti Teknologi MARA, Cawangan Negeri Sembilan, Kampus Kuala Pilah,
72000 Kuala Pilah, Malaysia
[4]Industrial Biotechnology Research Center SIRIM Berhad
No 1, Persiaran Dato' Menteri Section 2, PO Box 7035 40700 Shah Alam, Selangor
[5] Department of Chemistry,
Faculty of Science,
Universiti Putra Malaysia, Serdang, Selangor, Malaysia
[6] Biotechnology, Microbiology and Environment Collaborative Sciences,
Universiti Teknologi MARA, Cawangan Negeri Sembilan Kampus Kuala Pilah,
72000 Kuala Pilah, Negeri Sembilan, Malaysia

[*]Corresponding author: normonica@gmail.com , jafar@upm.edu.my

Received: 27 January 2022; Accepted: 10 June 2022; Published: 27 December 2022

Abstract

Wet chemical synthesis has received much attention to develop a wide array of metal oxide nanoparticles (MONPs) due to its low production cost, simplicity, and ability to produce ultrafine products. In recent years, room temperature ionic liquids (RTILs) as a superior solvent, have managed to produce excellent properties of MONPs that are gaining attention due to excellent physical properties such as small particle size, high surface area, and high porosity. To date, the abundance of available data on MONPs can now be used by researchers to establish suitable methods for producing high-performance materials particularly to suit specific applications. However, there is very limited information on the synthesis mechanisms and common characterization methods used in the preparation of MONPs using RTILs. Therefore, this paper aims to provide a comprehensive review on the MONPs synthesis methods using RTILs via sol gel, hydrothermal, microwave assisted, ultrasonic assisted, and precipitation method alongside the characterization by spectroscopic and microscopic techniques. In this article, various fabrication methods to synthesize MONPs with different morphologies and sizes are reviewed. Also, a step-by-step approach on the mechanisms to improve MONPs properties and impacts of RTILs on the formation of MONPs is highlighted. Finally, the potential of MONPs as antibacterial and catalyst are discussed.

Keywords: characterisation, ionic liquid, synthesis, metal oxide

Abstrak

Sintesis kimia basah telah mendapat banyak perhatian untuk membangunkan pelbagai jenis nanozarah oksida logam (MONPs) kerana kos pengeluarannya yang rendah, kesederhanaan dan keupayaan untuk menghasilkan produk ultrahalus. Dalam beberapa tahun kebelakangan ini, cecair ionik suhu bilik (RTILs) sebagai pelarut unggul, telah berjaya menghasilkan ciri-ciri terbaik MONPs yang mendapat perhatian kerana sifat fizikal yang sangat baik seperti saiz zarah yang kecil, luas permukaan yang tinggi, dan keliangan yang tinggi. Sehingga kini, banyaknya data yang tersedia mengenai MONPs kini boleh digunakan oleh penyelidik untuk mewujudkan kaedah yang sesuai untuk menghasilkan bahan berprestasi tinggi terutamanya untuk disesuaikan dengan aplikasi tertentu. Walau bagaimanapun, terdapat maklumat yang sangat terhad mengenai mekanisme sintesis dan kaedah pencirian biasa yang digunakan dalam penyediaan MONPs menggunakan RTILs. Oleh itu, kertas kerja ini bertujuan untuk memberikan ulasan komprehensif tentang kaedah sintesis MONPs menggunakan RTILs melalui sol gel, hidroterma, dibantu gelombang mikro, dibantu ultrasonik, dan kaedah pemendakan di samping pencirian oleh teknik spektroskopi dan mikroskopik. Dalam artikel ini, pelbagai kaedah fabrikasi untuk mensintesis MONP dengan morfologi dan saiz yang berbeza disemak. Juga, pendekatan langkah demi langkah mengenai mekanisme untuk menambah baik sifat MONPs dan kesan RTILs terhadap pembentukan MONPs diserlahkan. Akhir sekali, potensi MONPs untuk menghalang bakteria dibincangkan.

Kata kunci: pencirian, cecair ionik, sintesis, logam oksida

Introduction

Metallic elements can be transformed using various techniques to metal oxides nanoparticles (MONPs) with unique properties such as high surface to volume ratio, reduced surface imperfections, and superior magnetic, optical, electrical, and catalytic capabilities that are correlated to their size and distinct than their bulk materials [1-5]. MONPs are trendy in various applications, namely the health industry [6], textiles industry [7], in the cosmetic industry as antimicrobial agents [8] and the photocatalyst field [9, 10]. The designation of an experimental procedure for the synthesis of MONPs is an important aspect of nanotechnology with a size range of 1 to 100 nanometres (nm) [11]. With these demands, remarkable researches have been performed to prepare a variety of MONPs from d and f blocks elements in the periodic table such as iron oxide (Fe_2O_3) [12], magnesium oxide (MgO) [13], manganese oxide (MnO_2) [14, 15], zinc oxide (ZnO) [16], titanium oxide (TiO_2) [17], copper oxide (CuO) [18], zirconium oxide (ZrO_2) [19], silica oxide (SiO_2) [20], cerium oxide (CeO_2) [21], samarium oxide (Sm_2O_3), lanthanum oxide (La_2O_3) , ytterbium oxide (Yb_2O_3), and scandium oxide (Sc_2O_3). In general, there are two types of strategies to produce MONPs:

i) Top-down method: physical approaches which involve the fragmentation of bulk material into smaller fine particles up to nanoparticle sizes. This method uses several techniques such as ion and ball milling [22, 23], laser ablation [24, 25], chemical vapor, and deposition pulsed-laser deposition [26]. Moreover, this method requires the availability of tools or instruments and a competent operator to perform the specific techniques.

ii) Bottom-up method: tailor-made process using biological method such as plant extract [27, 28], fungi [29], and chemical method such as precipitation [30, 31] , sol–gel [32, 33], hydrothermal [34, 35], and microwave-assisted synthesis [36]. This method offers several advantages including a narrow size distribution, minimal energy usage, low processing temperatures for thermolabile materials, and low cost [37]. Moreover, these methods control the size and structures of MONPs by initiating kinetic energy within the particles to prevent clusters from accumulating [38, 39, 40].

Among the available methods to synthesize MONPs, the chemical method provides promising strategies owing to simpler procedures, ability to control reaction temperature, and high reproducibility [41]. The chemical method involves four main stages which are the formation of precursor, nucleation, growth, and ageing processes that can be controlled to obtain the desired size and shape [42]. To synthesize MONPs using the chemical method, a strong fundamental understanding of the method is required. Chemical methods have gained prominence for the synthesis of MONPs because of their mono-dispersive and non-agglomerative properties, which could be achieved by stabilising MONPs with capping agents especially during the growth stages [43]. This is because Ostwald ripening tends to occur during growth stages as it is a thermodynamically spontaneous process that leads to

agglomeration of the MONPs [44].Therefore, stabilizers or capping agents are needed for the synthesis of small MONPs as a protective layer that shields the particles from each other. Currently, several types of capping agents have been reported for the synthesis of MONPs such as tri-*n*-octyl phosphine oxide, dodecyle amine [45], aniline [46], polyethylene glycol [47], tetraoctyl ammonium bromide [48], hybrid poly(ethylene glycol), polyvinyl alcohols [49], octylamine [50], and room temperature ionic liquids (RTILs) to control the size of the MONPs.

The desired properties of RTILs are in terms of viscosity, conductivity, density, and thermal stability which could be regulated by altering the length of the alkyl chain of cations [51]. The synthesis of MONPs using RTILs has been proven to be environmentally friendly because RTILs can be reused and recycled for another cycle [52, 53]. Furthermore, due to their non-volatility characteristic, RTILs do not contribute to air pollution, and are deemed suitable and safe for industrial applications. The utilization of RTILs as a capping agent in the synthesis of MONPs has gained the attention of researchers due to their ability to produce an aggregation-free-end product, mainly due to the ionic liquid stabilization [54-58]. This is due to: (1) the unique structure of RTILs, cationic-anionic layers from RTILs surrounding the MONPs can generate a great electrostatic force between the MONPs [59], (2) the double-layered RTILs offer electrostatic interactions that can prevent MONPs from aggregating by balancing van der Waals interactions between the MONPs [60], (3) the alkyl side-chains of RTILs stretching far from the MONPs surface lead to a secondary steric stabilization to block the MONPs from approaching each other [61], and (4) the stabilization approach which involves hydrogen bonding from inter RTILs structure and intra RTILs-MONPs surfaces that may improve the synthesis of MONPs [62]. Common RTILs used as capping agents in the synthesis of MONPs involve groups from imidazolium [63], ammonium [30], choline [64], and pyrrole based RTILs [30, 65]. The use of RTILs as a capping agent has been proven to solve the agglomeration problem that usually occurs during the synthesis of MONPs. RTILs have been proven earlier as effective stabilizing agents in the formation of silver NPs [66], cadmium sulphide quantum dots [67], and silver/copper oxide/bentonite nanocomposites [68]. Moreover, RTILs can be used as a capping agent to control the size and shape of MONPs by manipulating the alkyl chain of cations or anions to achieve controllable physical properties [69, 70].

Numerous literature reviews have been published by researchers dedicated to the synthesis of MONPs concerning the utilization of RTILs. In 2011, Abbot et al. [71] provided a critical review on the processing metal and MONPs using RTILs. However, the review covered the role of RTILs in the extraction method to gain high purity metal and MONPs via physical synthesis only. In addition, review articles by Prechtl 2013 [72] and Seitkalieva et al. [73] on the synthesis of MONPs in RTILs covered the catalysis application and did not include a detailed mechanism on the formations of these MONPs in RTILs. Furthermore, there is limited information appertain to the roles of RTILs as a capping agent in the formation of MONPs in the chemical method, especially during the four important stages. In 2017, He and Alexandridis [2] reviewed the utilization of RTILs in MONPs, focusing on the hybrid benefits of MONPs and RTILs in the catalyst, electrochemical, and separation applications, The article only focussed on the emerging applications for the hybrid MONPs dispersed in RTILs. Furthermore, besides the essential contributions of RTILs in a variety of synthesis techniques and their excellent potential, the performances of MONPs in RTILs via chemical method should be emphasized. Therefore, attention must be given to the synthesis of MONPs via chemical method since these materials with smaller size are in great demand in various applications.

The present work will review the progress of the chemical method to synthesize MONPs using RTILs to produce excellent performances of MONPs. Subsequently, the characterization of MONPs involving transmission electron microscopy (TEM), scanning electron microscopy-energy dispersive X-ray (SEM- EDX), X-ray diffraction (XRD), ultraviolet visible (UV-Vis), and Fourier transforms infrared (FTIR) will be discussed herein along with the impacts and influences of RTILs in the MONPs synthesis. This review highlights the applications of MONPs in several sectors including antibacterial, catalysts, and others applications.

A step-by-step approach on the formation of MONPs via RTILs

As an alternative to the conventional organic molecular solvents, RTILs are used as a capping agent in the synthesis of MONPs. A capping agent is defined as an amphiphilic molecule consisting of a polar head

and a non-polar hydrocarbon tail. Both parts depend on the effectiveness of the capping agent, where the non-polar tail interacts with the medium around it, while the polar head coordinates with the metal atom [74]. A brief mechanism on the formation of zirconium oxide (ZrO2) NPs has been explained in our previous study [75]. Figure 1 depicts the reaction of the capping agent towards MONPs during the synthesis where each MONPs is well separated, thus reducing the risk of agglomeration. Typically, the formation of precursor molecules occurs during hydroxylation and hydrolysis reactions, creating a metal of zero charges [37]. Whereby, the metal hydroxides that are formed (formation of M-OH, where M is the metal) then take part in the condensation reactions lead to the nucleation of the solid material [76].

Nucleation is the second step in the preparation of MONPs, where the nuclei or seeds function as a template for crystal growth [1]. For example, the addition of reducing agent sodium hydroxide (NaOH) into the metallic precursor (zirconium chloride, $ZrCl_4$) solution causes the metal ion of Zr^{4+} to reduce to metal atom (Zr^0), creating supersaturated zirconium hydroxide (Zr-OH) that subsequently undergo nucleation [77]. Having said that, it is very important to control the concentration of NaOH in this step as it can indirectly affect the production of MONPs. For instance, if a lot of OH^- is produced in a short period, the metal ions in the solution will quickly precipitate due to the high pH environment, causing the metal ions to only have a minimal contribution to MONPs growth, prohibiting further growth of the MONPs [78]. Following nucleation, MONP's growth continues until the concentration of the precursor reaches equilibrium based on solubility [76]. Diffusion determines the growth rate of the particle; whereby smaller particles have recorded a larger growth rate compared to larger particles.

Next, the change in particle size occurs due to the ageing step that involves coarsening of the particle or also known as the Ostwald ripening process. Ostwald ripening is defined as a thermodynamically spontaneous process where larger particles are more energetically favored than smaller particles. Therefore, smaller particles diffuse in a solution before attaching themselves to the surface of larger particles. This step decreases the amount of smaller particles that are present in the solution. Meanwhile, agglomeration tends to occur rapidly for larger particles because larger particles tend to grow inappropriately due to lower surface energy [79]. The outcomes of the effect of RTILs structure in the MONPs synthesis could be observed through the morphologies and shape of the materials. The impact of the type of RTILs utilized and the exact reaction conditions on the particle size and shape of ZnO NPs were recently described by Alammar and Mudring [80]. It was discovered that increasing the length of the cation alkyl chain results in the creation of nanospheres rather than nanorods. This was explained by the steric effect of the longer alkyl chains of the RTILs with the ZnO NPs surface interaction which inhibit the growth of the particles for their typical creation of nanorods. It was also described that the longer cation chain contributes to smaller particle size with a diameter of 100 nm rather than shorter alkyl chain with a diameter of 400 nm. This was also agreed by other researches that also synthesized ZnO NPs that the length of the alkyl chain affect the morphology, size, and shape due to the steric hindrance [81, 82]. Similarly, the study on CeO NPs synthesis in RTILs reported that an exchange in RTILs cations would lead to a different morphology such that methylimidazolium $(C_3mimOH)^+$ and trishexyltetradecylphosphonium $(P_{66614})^+$ produced spherical-like and nanosheet assembly with particles size smaller than 10 nm.

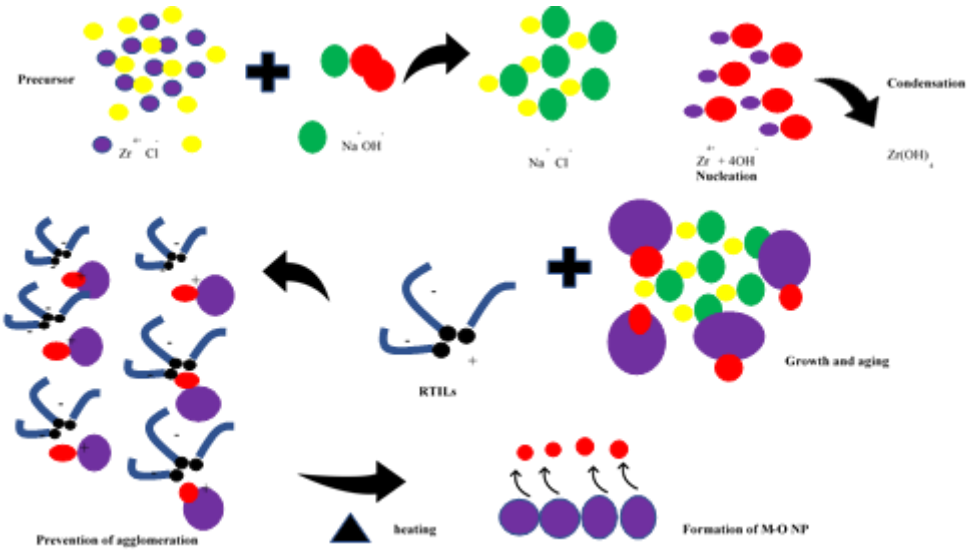

Figure 1. Proposed illustration for the steps in synthesis of MONPs using RTILs as capping agent. Source: [1, 37, 74-82].

Synthesis of MONPs using RTILs

Based on the evidence, the versatility of capping agents allows control over the agglomeration of particles from forming an anisotropic structure [83]. In addition, RTILs have been reported as effective capping agents in the synthesis of MONPs due to their peculiar structural properties. Therefore, the introduction of RTILs as a capping agent into the precursor solution allows the successful synthesis of many MONPs through bottom-up methods such as hydrothermal [84, 85], sol-gel [86], precipitation [30], microwave-assisted [36], and ultrasound-assisted [78] and their application as tabulated in Table 1. Of which, hydrothermal and sol-gel methods are most preferred because they are simpler and milder compared to microwave-assisted which requires special equipment to perform. In addition, sol-gel method is a green synthesize method that enables the recycling of RTILs, thus reducing the amount of chemicals used.

Table 1. Summary on methods and effects of RTILs on structure, properties, and application of MONPs

Method	RTILs	MONPs	Finding	[a]Size (nm) [b]Morphology	Application	Ref.
Sol-gel	Aliquat HTA-1	MnO_2	Good charging and discharging behavior at various current densities.	[a]20 [b]nanorod	Supercapacitor	[33]
	EMIMBr	TiO_2	The ratios of rutile to anatase in the products can be contro lled by altering the RTILs co ncentration.	[a]3.6-5.2 [b]nanorod	n.a	[32]
	$BMIMBF_4$	CeO_2	The formation of MONPs are successfully formed in RTILs acting as a soft-templating agent.	[a]15-20 [b]spherical	Auto-catalytic regenerative	[87]
	BMIMI	ZnO	May act as a template and very impactful on the structure and surface properties of ZnO NPs.	[a]9.13 [b]hexagonal	Antibacterial	[86]
	$BMIMBF_4$	MgO	RTILs formed an extended and lightly structured hydrogen bond network.	[a]30-50 [b]nanorod	n.a	[88]
	$BMIMPF_6$	TiO_2	Important in achieving a longer aging time for the formation of a stable sol-gel network.	[a]5 [b]sponge-like pore	n.a	[89]

Method	RTILs	MONPs	Finding	[a]Size (nm) [b]Morphology	Application	Ref.
	BMIMCl	Si-GO	Higher surface area with high crystalline phase.	[a]20-30 [b]spherical	Removal of heavy metal ions from water	[63]
	Benzimidazolium	ZnO	Good photocatalyst and antibacterial behavior.	[a]96.24 [b]n.a	Antibacterial	[90]
	$BMIMPF_6$	Nd_2O_3	Nd_2O_3-RTILs exhibited bactericidal activity yet at low concentrations and it is more effective drug for biomedical applications.	[a]48 [b]spherical, cubic, cuboic	Antibacterial	[91]
	TMPA-TFSI	Ag/Mn_3O_4/bent	Exhibited non-aggregated and displayed a significant amount of rod and spherical morphologies.	[a]10.4 [b]rod-like	Antibacterial	[92]
	$BMIMPF_6$	SrO/CeO_2	Controlled size of SrO/CeO_2 mixed MONPs exhibit antibacterial and antioxidant activity.	[a]5-55 [b]nanorod	Antioxidant and antibacterial	[93]
	$BMIMPF_6$	Ag-Au/Y_2O_3	RTILs controlled the growth and prevent the agglomeration of metal ions that give higher antibacterial and anticancer properties.	[a]30 [b]nanoflake=like	Biological	[94]
Hydrothermal	$BMIMBF_4$	Yb_2O_3	Less agglomeration due to the use of RTILs in the synthesis.	[a]35 [b] hexagonal, spherical, rectangular	Biological	[95]
	$BMIMPF_6$	Ag-rGO	Higher yields and better control over the diameter of the nanoparticles.	[a]10 [b] n.a	n.a	[96]
	TFSI	ZnO	Exhibited hexagonal shaped ZnO NPs in a very short period of reaction time.	[a]1500-2000 [b]hexagonal	n.a	[34]
	C_{16}MMIMBr	PtAg/rGO	Exhibited enhanced electrocatalytic performance, high methanol tolerant activity, and improved stability.	[a]31.5 [b]flower-like	Oxygen reduction	[97]
	$C_{10}MIMBF_4$ BMIM BF_4	ZnO	Difference alkyl chain length could affect the size of pore channels of hollow structure, the dispersivity and uniformity of ZnO NPs	[a]10 [b]ring-like	n.a	[98]
	C_3MIMBr	ZnO	Successfully synthesized ring-like ZnO NPs and promoted growth of tube-like structure.	[a]500 [b]ring-like hollow	Photoluminescence	[35]
	BDMIMCl	γ-Al_2O_3	Various morphologies successfully synthesis.	[a]90 [b]nanoleaves	n.a	[99]
	$BMIMPF_6$	Sm_2O_3	Particles are separated by distance without agglomeration.	[a]30-50 [b]cubic	Biomedical	[100]
	$BMIMBF_4$	WO_3	RTILs are important in the controlled synthesis of nanostructured materials.	[a]36 [b] spherical	NO_2 sensing	[85]
	HMIMBr	CeO_2– TiO_2	Large specific surface area and uniform pore size.	[a]3-4 [b]spherical	Photocatalytic	[101]

Method	RTILs	MONPs	Finding	[a]Size (nm) [b]Morphology	Application	Ref.
	BMIMCl	Fe_2O_3	Various morphologies of product yield.	[a]39.1 [b] hexagonal	n.a	[84]
	$BMIMBF_4$	TiO_2	Can prevent the production of brookite and favour the growth of the anatase phase.	[a]7.8 [b]n.a	Photocatalytic	[102]
	$BMIMBF_4$	ZnO	ZnO NPs with snowflake shape obtained as the RTILs used acted as a template which improved the sensitivity of NO_x sensor.	[a]600 [b]needle-like	Detection of NOx	[103]
	$BMIMPF_6$	La_2O_3	RTILs acts as a size and shape-directing agent contributes to good antibacterial and anti-inflammatory activities	[a]43 [b]spherical	Biomedical	[11]
Ultrasound-assisted	$EMIMBF_4$	Fe_2O_3	High conductivity with slightly increased viscosity and density.	[a]2-6 [b] quasi-spherical	Liquid marble	[78]
	$HMIMNTf_2$	ZnO	High yield and uniform diameter of small MONPs.	[a]60 [b]spherical	n.a	[104]
	Ionic liquid choline serinate	CeO_2	RTILs provide more stability to the MONPs and acts as cross-linking agent for collagen stabilization.	[a]19.95 [b]n.a	Biomedical	[105]
Precipitation	Poly (N- vinyl pyrrolidone)	ZnO	Increased efficiency in removing water pollutants.	[a]41.4 [b]spherical	Water treatment	[30]
	$BMIMNTf_2$	Fe_2O_3	MONPs exhibited well-controlled size and size distribution.	[a]10.6 [b]spherical	n.a	[31]
Microwave-assisted	$OMIMPF_6$	ZnO	No agglomeration, pure product.	[a]16 [b]spherica	Esterification reaction	[36]

1-ethyl-3-methyl-imidazolium bromide (EMIMBr), neodymium oxide (Nd_2O_3), N-trimethyl-N-propylammonium bis(trifluoromethanesulfonyl)imid (TMPA-TFSI), silver/manganese oxide/bentonite (Ag/Mn_3O_4/bent), lithiated sarcosine-trifluoromethyl sulfonyl imide (TFSI), silver nanoparticles-reduced graphene oxide (Ag-rGO), 1-hexadecyl-2,3-dimethylimidazolium bromide (C_{16}MMIMBr), bimetallic reduced graphene oxide (PtAg/rGO), 1-decyl-3-methylimidazolium tetrafluoroborate ($C_{10}MIMBF_4$), 1-propyl-3-methylimidazolium bromide (C_3MIMBr), 1-butyl-2,3-dimethyl imidazollium chloride (BDMIMCl), gamma-aluminium oxide (γ-Al_2O_3), lanthanum oxide (La_2O_3), Silver and gold decorated Y_2O_3NPs (Ag-Au/Y_2O_3), graphene oxide (GO), silica–graphene oxide nanocomposite (Si-GO), 1-ethyl-3-methylimidazolium bis (trifluoromethylsulfonyl)imide (EMIMTFSI), 1-butyl 3-methyl imidazolium Iodide (BMIMI)., n.a (not availbale).

Sol gel method

Among many available methods, sol-gel is an effective and the simplest chemical method to synthesize MONPs with the desired properties. This method involves various steps starting with the hydrolysis process, followed by polycondensation, gelation, and aging of the metal alkoxide in the presence of acid or base. From this mechanism, a pure and homogenous product would be formed in mild condition before subjected to drying, compaction, and crystallization steps that would improve the chemical homogeneity of the MONPs formed [106, 107]. The reaction of sol-gel through partial hydrolysis of the alkoxide, polycondensation of the hydroxyl, and polymerization of alkoxyl groups are explained using equations as follow [108]:

$$M(OCH_2CH_3)_{10} + x6H_2O \rightarrow M(OCH_2CH_3)_4(OH)_6 + 6CH_3OH \quad (1)$$

$$M\text{-}OH + HO\text{-}M \rightarrow M\text{-}O\text{-}M + H_2O \quad (2)$$

$$M\text{-}OCH_3 + HO\text{-}M \rightarrow M\text{-}O\text{-}M + CH_3OH \quad (3)$$

Fang and Song [87] synthesized CeO_2 NPs via the sol-gel method using cerium nitrate hexahydrate ($Ce(NO_3)_3.6H_2O$) as a precursor dispersed in water. During the synthesis activity, a capping agent of $BMIMBF_4$ was added to control the formation of MONPs. The RTILs in the supernatant solution was collected using a rotary evaporator and was reused in the next synthesis activity of CeO_2 NPs. The recycled

activity indicated that the capping agents used were environmentally friendly. The size of the obtained CeO_2 was between 15 nm to 25 nm after calcined at high temperature for 6 hours. The research was then expanded to study the formation of CeO_2/Chitosan composite. According to the UV-visible spectrum, adding cerium oxide nanoparticles to the chitosan polymer produced a high ability of catalytic oxidative recovery from spectrum shifting, which could be related to the material's tiny size which allowed the penetration into chitosan.

Pandiyan et al. [93] reported a simple and eco-friendly method using RTILs which assisted green synthesis of ceramic SrO/CeO_2 NPs via the sol-gel method. The prepared SrO/CeO_2 NPs were highly crystallized and purified when analyzed using XRD. Based on the investigation, the $BMIPF_6$ improved the surface morphology of the SrO/CeO_2 NPs as compared to the synthesis without BMIM]PF_6. This was due to the material that was uniformly distributed, and the growth and agglomeration activities that was controlled with the presence of $BMIMPF_6$.

Meanwhile, Sundarajan et al. [86] successfully prepared nanocrystalline ZnO NPs using the sol-gel method using 1-butyl 3-methyl imidazolium iodide ($[BMIM]^+ I^-$) as a capping agent. The product was calcinated at 400 ℃ to produce white colored ZnO NPs. To overcome the drawback, $[BMIM]^+ I^-$ was added which acted as a capping agent by adsorbing on the surface and covering the ZnO NPs during crystallization. The calculated average crystal size was found to be smaller with the presence of $BMIM]^+ I^-$ than that without RTILs, indicating the significant role of ($[BMIM]^+ I^-$) in influencing the structure and surface properties of ZnO NPs. During the application of ZnO NPs as an antibacterial agent, it was observed that the bacterial growth inhibition increased due to their small particles size and improved morphology which improved the uniform distribution of Zn^{2+} ions on the bacterial surface, indicating significant enhancement of antibacterial activity. In recent years, Sundarajan et al. [91] reported on the advanced synthesis of neodymium oxide nanoparticles using the sol-gel method by reacting neodymium chloride hexahydrate ($NdCl_3.6H_2O$) and $BMIMPF_6$ at room temperature. The final product was calcinated at a very high temperature (650 ℃) for 5 hours in a muffle furnace. As a result, a material highly improved surface smoothness was obtained due to the excellent roles of the capping agent ($BMIMPF_6$) to control the particles agglomeration as compared to the materials without RTILs. Moreover, they reported that the scavenging activity of Nd_2O_3 NPs synthesized in $BMIMPF_6$ was higher than that of Nd_2O_3 NPs, suggesting that they could be exploited as a viable treatment of diabetes disorders.

On the other hand, a similar method was investigated by Bharate et al. [33] to synthesize MnO_2 NPs in Aliquat HTA-1, whereby 1.5 g of manganese chloride (precursor) was dissolved into 25 mL of distilled water before the addition of Aliquat HTA-1. During the synthesis of MnO_2 NPs, weight ratio of MnO_2 NPs to Aliquat HTA-1 of 1:4 was added amidst the synthesis to ensure that all the particles were capped with the RTILs as it prevents agglomeration, which further prevents anisotropic growth of the particle. The amount of RTILs added was larger than most reported literature that used imidazolium based RTILs. In their work, a comparison study to investigate the effectiveness of RTILs was done where one of the MnO_2 NPs was synthesized without RTILs showing to form spherical shape in contra to nanorods. The RTILs used in this study was also used as an electrolyte during the supercapacitor application where they used 5% of Aliquat HTA.

Hydrothermal method

The hydrothermal method is another choice of method to synthesize MONPs that typically use Teflon-line stainless steel autoclaved reactor with temperature higher than 100°C and pressures above 1 atm [109]. Liu et al. [101] used RTILs to synthesize CeO_2 NPs. It was done by dissolving 0.005 mol of 1-hexadecane-3-methylimidazolium bromide ($C_{16}MIM^+Br^-$) in 15 mL distilled water through vigorous stirring at 40°C for 30 minutes. Then, tetrabutyl orthotitanate (TBOT) and cerium nitrate ($Ce(NO_3)_3$) were added to the solution. In their study, they reported for the first time a facile synthesis of hybrid MONPs of CeO_2–TiO_2 NPs with adjustable Ce/Ti percentages using RTILs, where the molar proportion of cerium (Ce) in the composition varied in the range of 5% to 30%. Upon the completion of stirring for 30 minutes, the pH of the solution was adjusted to 9 -10 using dropwise addition of ammonia solution followed by stirring for 2 hours. Then, the homogeneous sol was transferred to a 100 mL Teflon-line stainless steel autoclave at 100°C for 2 days. The finding from XPS spectra revealed that the Ce^{3+}concentrations decreased from 5% CeO_2–TiO_2 to 30% CeO_2–TiO_2 , indicating that the amount of Ce^{3+} in total Ce declined with the growing amount of CeO_2

NPs.

Zhang et al. [85] investigated the role of RTILs in improving the sensitivity of tungsten trioxide (WO_3) to NO_2 gas. In the synthesis of the material, different concentrations of $BMIMBF_4$ were added amidst the synthesis process. The surface composition of the material was studied using X-ray photoelectron spectroscopy (XPS), which revealed characteristic peaks corresponding to the C, O, W, and N elements in the materials, as well as the appearance of a N 1s peak at 400.2 eV, attributed to imine (=N-) derived from the imidazole ring in RTILs. When compared to WO_3 NPs generated without the addition of RTILs, the as-synthesized WO_3 NPs have significantly enhanced the sensing characteristics of NO_2. The phenomenon could be attributed to the high proportions of surface adsorption oxygen and the residue of C-N from $BMIMBF_4$, thus creating a large specific surface area.

On the other hand, Muthulakshmi et al. [100] used the same hydrothermal method in the synthesis of samarium oxide (Sm_2O_3) NPs. In their work, they utilized 1-butyl 3-methylimidazolium hexafluorophosphate ($BMIMPF_6$) to assist the synthesis route. In their findings, the particle size Sm_2O_3 NPs was between 50 nm and 80 nm as examined using dynamic light scattering method. Due to the superior properties of $BMIMPF_6$ as a capping agent, the particles were found well separated by a certain distance without agglomeration. The consistent particle size distribution and surface charge distribution visible in this finding could possibly explain the stability of Sm_2O_3 NPs produced in $BMIMPF_6$. Subsequently, the stability of the MONPs was proven by a high zeta potential (36.3 mV), indicating high stability of the synthesized Sm_2O_3 NPs. In the recent year, Muthulakshmi et al. [110] described the synthesis of ytterbium oxide (Yb_2O_3) NPs using the same capping agent ($BMIMPF_6$). It was discovered that the large agglomeration of NPs was minimized due to the addition of $BMIMPF_6$ in the synthesis process which was evidenced by using a particle size analyzer. The polydispersity index (P.I.) of the material was calculated to be 0.246 along with the superior electrophoretic mobility (0.000212 cm_2/Vs), indicating a homogeneous particle size distribution and surface charge. Furthermore, the stability of Yb_2O_3 NPs was excellent, making the potential of the material in medicinal field possible.

Microwave-assisted method

The microwave assisted method uses a domestic microwave oven to synthesis MONPs that involves efficient heating method which can significantly decrease the reaction time by the operation of electromagnetic waves between 300 MHz to 300 GHz [54]. For example, Kavya et al. [36] explored the microwave-assisted method to prepare ZnO NPs. 16 g of NaOH was added to 5.5 g zinc acetate dihydrate and 50 mL of distilled water while stirring. The suspension was placed in a microwave oven after adding 2 mL of $OMIMPF_6$ to 3 mL of the prepared solution (2.45 GHz, 850 W). The mixture was then irradiated for 2 minutes to 9 minutes in a loop using 30% of the microwave's output power (on 10 s; off 5 s). The formed spherical shape of the ZnO NPs was discovered to be greatly controlled by the initial production of nuclei by microwave irradiations, and then the subsequent role of the ionic liquid as a growth controller. A small particle size (16 nm) of ZnO NPs was obtained, making them suitable as a catalyst in the esterification between benzoic acid and methanol. The esterification reaction using 5 mol% ZnO NPs as an acid catalyst provided excellent yields in a short reaction time (2 hours), indicating that the produced ZnO NPs have outstanding potential as an alternative catalyst. The microwaved assisted method of MONPs synthesis in addition of RTILs as a capping agent can act as a microwave absorber and improve the induced uniform heating into the solution and maintain thermal homogeneity by an ionic conduction mechanism that lead to the formation of MONPs [42].

Precipitation method

Precipitation method is another synthesis method that is unique, cost-effective, simple, and involves controlling the pH of the medium [111]. The precipitation reaction process consists of five steps[112]:

(1) Dissociation of NaOH: $2NaOH_{(s)} \rightarrow 2Na^{+}_{(aq)} + 2OH^{-}_{(aq)}$

(2) Dissociation of precursor: $M(NO_3)_2{\cdot}XH_2O_{(s)} \rightarrow M^{2+}_{(aq)} + 2NO_3^{-}{}_{(aq)} + XH_2O$

(3) Formation of metal hydroxide: $M^{2+}{}_{(aq)} + 2OH^{-}_{(aq)} + XH2O_{(aq)} \rightarrow M(OH)^2{\cdot}XH_2O_{(s)}$

(4) Formation of colorless solution: $2Na^{+} + 2NO_3^{-} \rightarrow 2NaNO_3$

(5) Drying: $M(OH)_2{\cdot}XH_2O_{(s)} \rightarrow Zn(OH)_{2(s)} + XH_2O_{(g)}$ and

(6) Calcination: $M(OH)_{2(s)} \rightarrow MO_{(s)} + H_2O_{(g)}$

For instance, Atta et al. [30] synthesized ZnO NPs using the precipitation method. In brief, zinc nitrate hexahydrate (0.1 mol) was dissolved in 50 mL water and mixed with 4 g of poly-2-Acrylamido-2-methyl-1- propane sulfonic acid (PAMPSA) or poly-2-Acrylamido-2-methyl-1-propanesulfonic acid/N-vinyl pyrrolidone (PAMPSA/VP) under intense stirring until a clear solution was obtained. Then, 30 mL of NaOH (0.2 M in ethanol) was added to the reaction mixture and vigorously stirred until the pH of the solution reached 12.5. The pH is one of the important factors to be monitored as it has an impact on the product obtained. The number of H^+ or OH^- ions in the sol, which effectively dictates the polymerization of the metal–oxygen bonds, is well recognized to have a substantial influence on the morphology of the produced metal oxide precipitation/solution. The hydrolysis and condensation behavior of the solution during gel formation is affected by the pH of the precursor solution, thus affects the shape but does not affect much on the crystal quality of the MONPs [113]. Therefore, it is important to make sure the solution reach the desired pH to obtain the desired MONPs. Next, to produce a milky solution, the reaction temperature was increased to 45°C for 4 hours before letting it to rest. Then, the cooled reaction mixture was centrifuged at 15000 rpm for 10 minutes. To extract the aggregates and organic impurities, the precipitate was washed several times with distilled water and ethanol before drying for 5 hours at 150 °C.

Ultrasound-assisted method

The ultrasound-assisted method is a method that uses ultrasonic irradiation at frequencies ranging from 20 kHz to 500 MHz in sonochemical technologies to begin or modify chemical processes [54]. This method was described in two different studies to synthesize Fe_2O_3 NPs and ZnO NPs. For example, Zhang et al. [78] described the synthesis of Fe_2O_3 NPs through facile and energy saving (100 mW) ultrasonic decomposition of $Fe(CO)_5$ with 20 ml of $EMIMBF_4$ in a 50 mL round-bottomed flask in an ice bath. The ultrasound probe was placed 1 cm below the liquid surface, where the mixture was ultrasonicated for 1.5 hours at 100 mW. It was discovered that steric forces successfully stabilized the colloidal particles in $EMIMBF_4$, since the bulky structure of molecules/ions $EMIMBF_4$ strongly attached to the colloidal surfaces, allowing them to separate each colloidal surface in some circumstances. The nonpolar alkyl chains acted as a protective group and further inhibit the aggregation of the particles. Similarly, $EMIMBF_4$ enhanced the solvation force in the generation of MONPs, where the multi-layered structure created longer range repulsion and minimized agglomeration.

Whereas, Goharshadi et al. [104] prepared ZnO NPs by dissolving zinc acetate dihydrate into distilled water with dropwise of NaOH solution. The synthesis activity was magnetically stirred under room temperature, resulting in a clear $[Zn(OH)_4]^{-2}$ solution. Before subjected to 40 kHz of ultrasonication for 1 hour, HMIMNTf2 was added into the $[Zn(OH)_4]^{-2}$ solution until white precipitate of ZnO NPs was obtained. The total acoustic power injected into the sample solution was estimated at 50 W by a calorimetry. The white ZnO NPs precipitate was then centrifuged, washed, and dried for 10 hours in a vacuum oven at 40 °C. According to the analysis, both HMIMNTf2 and ultrasound posed a critical role during the formation of ZnO NPs. The obtained ZnO NPs were spherical in shape and well aggregated, consisting of numerous tiny nanoparticles with homogeneous diameters of about 60 nm. This could be possibly explained through the capping agent of HMIMNTf2 which consists of cation $[C6mim]^+$ and anion $[NTf2]^-$. Cation from $[C6mim]^+$ created the electrostatic attraction within the precursor solution comprising a large number of $[Zn(OH)_4]^{2-}$ ions. Due to the high polarization of $[C6mim]^+$, these cation–anion pairs were likely to dehydrate and produce ZnO NPs nuclei. Furthermore, $[C6mim]^+$ ions containing hydroxyl can still adsorb the negatively charged ZnO NPs nuclei's surface to restrict the activities of freshly produced ZnO NPs surfaces, causing the anisotropic development of ZnO NPs to be significantly controlled. The features and comparative analysis of different chemical synthesis methods for MONPs is displayed in Table 2.

Table 2. Comparative analysis of different chemical synthesis methods for MONPs

Synthesis Method	Specific Features	Advantages	Disadvantages
Sol gel method	1. A sol (or solution) grows slowly to form a gel-like system containing liquid and solid phases [114].	1. Possible recycling of RTILs. 2. Made at considerable low temperature below 100 ºC.	1. Product controlled by various parameters; where the final product obtained is affected by concentration of precursor, pH condition, and synthesis time during the sol-gel reaction [115].
Hydrothermal method	1. The action of water at elevated pressure and temperature under a sealed environment in an autoclave [116].	1. Highly nanostructured nanoparticles are controlled over pressure and temperature only [117]. 2. Zero-emission of toxic gases, since the reaction are in the closed system of autoclave [118].	1. Requires expensive equipment (autoclave).
Microwave-Assisted Method	1. Open vessel is simpler than closed vessels [119]. 2. The absorption of microwave radiation by the precursor followed by heat generation through dielectric heating [120].	1. Uniform heating. 2. Possible to use household microwave oven [121]. 3. Use scientific microwave oven. 4. Heats the target molecules directly. 5. Very short reaction time and high efficiency.	1. Requires expensive equipment (microwave oven).

Synthesis Method	Specific Features	Advantages	Disadvantages
Precipitation method	1. Synthesis begins with reaction between metal and alkaline solution or precipitating agent (NaOH, KOH, ammonia etc.) followed by aggregation and precipitate product is collected by filtration or centrifugation [122].	1. Simple. 2. Shape of the particle can be alter by changing the precursor, type of precipitating agent and quantity of organic phase [123]. 3. High crystallinity and homogeneity of product [124]. 4. Cost-effective and scalable [125].	1. pH sensitive. 2. Further thermal treatment is needed [122].
Ultrasound-assisted method	1. Involves energy in the form of heat, light, radiation, electric potential [126]. 2. Formation of bubbles due to the cavitation during ultrasonication [127].	1. More appropriate method for green and sustainable synthetic processes [128]. 2. Minimization of waste [129]. 3. Effective for nanoparticle formation as it yields high product.	1. Require expensive equipment (ultrasonic irradiation). 2. Various reaction parameters including temperature, time, energy input, and pressure must be controlled [126].

Characterization

Morphology and microscopy analysis

Microscopy analysis by transmission electron microscopy (TEM) and scanning electron microscopy (SEM) are carried out to study the morphology of MONPs such as quality, shape, density, diameter, thickness, length, size, and orientation of the as-grown nanostructure [130]. Both use a beam electron to view an image, whereby TEM image is displayed in a two-dimensional projection that passes through the sample while SEM image illustrates the surface morphology of the sample [131, 132].

Scanning electron microscopy

SEM is a microscopy technique that focuses the electron beam to a spot and interacts with the sample which then produces various signals that are combined to form an image. The formation of the image can be used to obtain information about the surface topography and composition depending on the scan pattern chosen [133]. In assessing the physical properties of MONPs, SEM imaging techniques are usually employed to observe their microstructure and morphological properties like size and shape distribution.

A previous study by Mahjoub et al. [134] who synthesized ZnO NPs using chiral ionic liquid (2[N-(n-But)$_4$]+[$C_2H_4(OH)_2(CO_2)_2$]$^{2-}$) (CIL) as a capping agent proved that the absence of CIL resulted in the agglomeration of flower-like ZnO NPs as demonstrated by the obtained SEM image. This shows that CIL plays an important role in morphology of the ZnO NPs. As for the growth of flower-like crystal, when [Zn $(OH)_4]^{2-}$ was decomposed, oxide nuclei developed quickly and served as the growth unit for the formation of ZnO NPs nuclei and epitaxial growth into the flower-like structures. This phenomenon can occur with the help of microwave heating. In general, each Zn^{2+} atom is surrounded by a tetrahedral group of four oxygen ions in hexagonal packing, making the CIL cations and anions easily absorbed on the of O^{2-} and Zn^{2+} surfaces by electrostatic force. However, the amount the CIL extensively affected the morphology of the ZnO NPs as the CIL presence was at 0.3 g, resulting in a narcis-like morphology of the ZnO NPs. A similar finding was also obtained by Kowsari and Karimzadeh [135] who synthesized BaO NPs using CIL, where the amount of CIL added into the MONPs affected the morphology of the product such that a low amount of CIL (0.15 g) formed a heterogenous butterfly-like and cubic like morphology while a higher amount of CIL (0.25 g) formed a cubic like morphology. Instead, they reported that decreasing concentration of CIL reduced the amount of ion carrying the OH group that were responsible for the growth of BaO NPs nuclei to navigate the surfaces forming both cubic and butterfly-like morphologies.

EDX analysis

The elemental mapping using EDX analysis is particularly important in proving the presence of metallic elements and other elements such as oxygen in the sample. This technique can be considered as qualitative and semi-quantitative analysis. The intensity of the peaks in the spectrum indicates the concentration of the respective element since every element has a specific set of peaks in the photoelectron which is determined by photon energy and the respective binding energies [136]. A study on the synthesis of silver NPs using three biodegradables protic ionic liquid (PILs) was reported by Tzani et al. [137], whereby the EDX spectra indicated the composition of the important elements. According to the EDX spectra, the Ag particle was the major element present in the composition with zero interruption from nitrogen element indicating that the NO_3^- ions were appropriately washed and perhaps it did not cap or adsorb in the Ag particles. Indeed, the PILs were successfully washed away using acetone, ethanol, and water. However, it did not interfere with the formation of the Ag NPs [137]. Similarly, a notable evidence of study specifically related to the EDX spectra of CeO_2/ZrO_2 core MONPs synthesized with $BMIMPF_6$ showing a well homogenous composition of cerium (25.95%), zirconium (8.325%), and oxygen (12.07%) due to the washing step during the synthesis using distilled water prior to the characterization technique [138]. However, they also emphasized on the significance of calcination of the MONPs core since the sintering of the particles would give a homogeneity of the MONPs product. Furthermore, another study [95] revealed similar results to the previous study where pure Yb_2O_3 NPs was synthesized using $BMIMPF_6$ in which the elemental composition percentages of ytterbium and oxygen peaks were 85.5% and 10.1%, respectively.

Transmission electron microscopy

TEM is used to observe the size distribution and morphology of the MONPs powder [139]. This analysis provides crystal or surface structure information along with the image up to a few angstrom resolutions. Determination of chemical composition is made possible when TEM is equipped with EDX since the working principle of TEM uses a high energy electron source of around 200 KeV [130]. A thin sample is irradiated with an electron beam of uniform current density passes through the samples to help visualize the size, shape (spherical, flower-like, rod-like or spindle-like structure), and effects of agglomeration [88]. Valuable information on the shape and particle size can provide the potential activity or quantify the distribution characteristics [140]. Moreover, the advantages of TEM include the ability to display the agglomeration of particles under a high-resolution image [141, 142].

As an alternative solvent to improve the properties of the MONPs, RTILs were used as capping agents in several studies [30, 33, 36, 78, 143]. Morphology of ZnO NPs synthesized using (TBA_2($_L$-Tar)) RTILs was elucidated using TEM that proved a flawless rose-like structure and were made up of self-assemble nanosheets with a length and width of several micrometers and a thickness of 30–40 nm with a preferred orientation due to the effect of tartrate anions that reformed the growth mechanism of the ZnO NPs [144]. This confirm that the CIL presence in the synthesis proscribed the 1D growth of the ZnO NPs nanostructures and rearranged the ZnO NPs to form 2D nanosheets that assemble into the hierarchical architectures like "roses." However, the author mentioned, generally the uses of basic imidazolium-based RTILs tends to formed a typical ZnO NPs in nanorods or nanowires structures based on the anisotropic growth of the crystal. In other words, RTILs can be soft templating to the formation of the MONPs structure that can be confirmed by TEM. This finding was found similar in other study where the CIL was acting as template in the formation of ZnO NPs and CuO NPs and the morphology reported a flower-shape with the particle size in the range of 100 – 200 nm for ZnO NPs and a needle-like shape for CuO NPs with a length of 400 – 500 nm and a diameter of 10 – 15 nm. Although the MONPs was synthesized using CIL, there was no significant change in morphology but when the CIL was not added in the MONPs synthesis, the TEM image showed an irregular size and shape. Probably, the presence of RTILs even as a simple additive in water can indeed affect the morphology of CuO NPs. This might be due to the strong electrostatic interactions between anions and cations, as well as π-π stacking and van der Waals interactions involving imidazolium cations perhaps can influence the formation of MONPs that are further characterized using TEM [145].

Moreover, $BMIMPF_6$ is one of the common RTILs used in the synthesis of MONPs to act as capping agent in order to prevent the agglomeration of the MONPs. A Previous study used $BMIMPF_6$ in the synthesis Nd_2O_3 NPs exhibited cubic and spherical shape with a diameter of 48 nm. The synthesis of Nd_2O_3 NPs was reported to exhibit more effective drug delivery for biomedical application [91]. Similarly, Pandiyan et al. also used the same RTILs to control and prevent the agglomeration of metal ions that contributed to nanoflake-like structures of Ag-Au/Y_2O_3 NPs with a diameter of 30 nm. The MONPs obtained were also suitable to be applied in antibacterial and anticancer applications [94]. In addition to this, Veerasingam et al. and Muthulakshmi et al. also reported a size of 43 nm and 50 nm for La_2O_3 NPs and Sm_2O_3 NPs, respectively based on their TEM micrographs. From the TEM image, the crystalite size of La_2O_3 NPs in the absence of $BMIMPF_6$ clearly showed agglomerated particles and while RTILs assisted of La_2O_3 NPs showed agglomeration free particles. Both study reported that $BMIMPF_6$ was able to act as shape-directing agent and the particle were well separated without any agglomeration [11, 100]. It is worth to point out that, $BMIMPF_6$ was suitable in synthesis of various MONPs as this RTIL have weak interaction of cation and anion when interacted with water that enabled the positively charged metal ions to interact with the negatively charged of the RTILs anion to control the growth of the MONPs. From the reported journal, it was noted that a morphology, size, crystal structure, qualitative, and quantitative analysis can all be done using these characterization techniques as this technique provides higher resolution than a light microscope [146].

Besides that, another alternative of RTILs used to prevent agglomeration of the synthesized MONPs was mentioned in previous study by Liu et al. [147] who used 1-hexadecane-3-methylimidazolium bromide (HMIMBr) as a template via the hydrothermal method to produce well-dispersed CeO-TiO_2 NPs. The TEM images demonstrated rod-like shape for 5% CeO-TiO_2 NPs, 10% CeO-TiO2, and 15% CeO-TiO_2 NPs, while

the spherical shape was observed for pure CeO NPs and 30% CeO-TiO_2 NPs at an approximate size of 15 nm. The prepared CeO-TiO_2 NPs was used in the photocatalytic degradation of p-chlorophenol that produced high photocatalytic activity under UV or visible irradiation [101].

Spectroscopic analysis

Fourier-transform infrared

FTIR spectroscopy is a technique used to obtain the absorption or emission spectrum of a solid, liquid or gas in the infrared region, where the spectrum promotes transition between the rotational or vibrational energy level of the ground electronic energy state [148]. Usually, FTIR is used to confirm the bonding and qualitatively detect the presence of functional groups in a nanostructure [139, 149]. FTIR spectroscopy is used to identify functional groups, main vibrational mode, impurities (if any), and determine the purity of MONPs that validates the structural unit and connectivity such as bridging and non-bridging of oxygen in the synthesis of MONPs [150, 151].

The synthesis of MONPs using RTILs has gained interest recently due to the advantages of RTILs. The interpretation of typical peak is still considered as highly divisive due to the difference in opinions expressed by many researchers. A slightly similar peak was almost found on every synthesis MONPs indicating the stretching vibration of O-H bond that are mainly from the alcohol residue. This statement was well supported by a few researchers that synthesized MONPs using RTILs. For instance, Nithya et al. who synthesised CeO_2/ZrO_2 NPs core synthesized using $BMIMPF_6$ reported a broad band at 3426 cm^{-1}. This was similarly found by Veerasingam et al. [11] who observed a broadband at 3453 cm^{-1}. However, Sundrarajan et al. indicated that a broadband located at 3437 cm^{-1} attributed to hydroxyl group of water molecule. Besides that, even though ZrO_2 NPs and CeO_2 NPs have typical absorption peaks at 600 cm^{-1} and 510 $cm^{-1,}$ respectively, the distortion of the peak was reported for CeO_2/ZrO_2 core synthesized using $BMIMPF_6$. The significant peaks were observed at 498 cm^{-1} (CeO_2 NPs) and 416 cm^{-1} (ZrO_2 NPs) mainly due to the effects of zirconia grafting on the cerium surface and was not affected by the $BMIMPF_6$ which enhanced the size and morphology of the MONPs without altering the environment [138]. This finding was then further supported by Fang and Song who synthesized CeO_2 NPs capped by $BMIMBF_4$, the FTIR spectrum manifested a single-phase crystalline CeO_2 NPs with band peaks at 640 cm^{-1} and 673 cm^{-1} representing the Ce-O-Ce stretching vibration. This study reported that the two peaks above 3000 cm^{-1} in the infrared (IR) spectra indicated diagnostic changes in the C-H-F hydrogen bonding between BF_4 anions and the position of hydrogen at 4,5 within the imidazolium ring [87]. This phenomenon revealed that the method employed to synthesize MONPs did not remove all RTILs, hence may require several modifications including calcination temperature and type of method to achieve excellent purity.

It was in contrary to another study that RTILS did not alter the significant functional group of MONPs as none of the RTILs peaks appeared in the FTIR for those MONPs synthesized in RTILs. Based on the results, peaks for Ag-Au doped RuO_2 NPs in $BMIMPF_6$ was determined at 476 cm^{-1} belonging to RuO_2 NPs [152]. Another peak identified in the spectrum corresponded to the hydroxyl group (O-H) indicating the presence of OH bonded alcohol and a phenolic compound that arose from the plant extract used in the synthesis of the MONPs [152]. Furthermore, Sundrarajan et al. [86] provided complementary results for the synthesis of ZnO NPs that reposted the finding of Zn-O stretching vibration at 418 cm^{-1} in the spectra. This study also reported the presence of several other peaks at 2956.97 cm^{-1}, 2404.04 cm^{-1}, 1764.93 cm^{-1}, 1388.00 cm^{-1}, and 1164.38 cm^{-1} indicating the presence of C–O and C–H stretching vibrations from the phenolic compounds within the plant extracts before calcination. While the peak at 1626.95 cm^{-1} maybe due to the presence of intramolecular hydrogen bonds of the ionic liquid. Following the calcination process, the peak at 3500 cm^{-1} remained due to O–H stretching vibration from moisture adsorption. In this study, ZnO NPs were synthesized with the absence and presence of BMIMI but the significant stretching vibration of Zn-O spectra appears at the same wavenumber whereby this indicate that the addition of the BMIMI does not alter the purity of the ZnO NPs. However, uses of another type of RTILs may contribute to peak shifting that may be attributed to changing properties of the synthesis ZnO NPs. For instance, the synthesis of ZnO NPs using chiral ionic liquid reported a strong adsorption peak at 544 cm^{-1} that can be assigned to the Zn–O stretching bonds. With comparison to the typical absorption spectra of ZnO NPs, this peak was shifted to a higher wavelength, and this feature

attributed speculatively to the distinctive structure of ZnO NPs formed in the presence of the RTILs [145].

On the other hand, in another study [99], FTIR was performed to assess the nature of bonds and absorbance of the peak in the prepared Sm_2O_3 NPs. A broad prominent peak was observed at 3444 cm^{-1} which corresponded to O-H stretching vibration, indicating the presence of a water molecule. While the absorption peaks at 1109 cm^{-1} indicated C-O stretching vibration. Also, significant peaks were observed at 749 cm^{-1} and 657 cm^{-1} for Sm-O stretching vibration. In summary, Table 3 lists the functional groups and wavenumber range for the MONPs discussed in this section.

Table 3. Main Functional Groups of MONPs and Wavenumber.

MONPs	Wavenumber (cm^{-1})	Vibrational Mode	Ref.
CeO_2	673	Stretching	[52]
	450	Stretching	[153]
	674 and 545	Stretching	[21]
ZnO	418	Stretching	[86]
	501	Stretching	[112]
ZrO_2	595	Stretching	[138]
	492.73	Stretching	[19]
	473	Stretching	[154]
TiO_2	490	Stretching	[155]

UV-visible spectroscopy

The UV–Vis spectra of MONPs provide significant information regarding their optical characteristics. UV–Vis spectroscopy is also used to investigate the defect energy states induced by various doping agents in MONPs [156, 157]. Besides, for MONPs, UV-vis is commonly used to characterize supported single MONPs and it is widely known that absorption edge energies reduce as oxide domain size increases [158].

Bharate et al. [33] reported that the MnO_2 synthesized with aliquat HTA-1 had a significant absorption at λ_{max} 395 nm that showed smaller bathochromic shift, whereas MnO_2 NPs prepared without aliquat HTA-1 had absorption at λ_{max} 386 nm which could be due to its size and form. The MnO_2 NPs with aliquat HTA-1 had a smaller bathochromic shift than MnO_2 without aliquat HTA-1, which could be due to its size and form. These results show that Aliquat HTA-1, an RTIL, functioned as a surfactant and regulated the size and form of nanoparticles. Similarly, the UV–visible spectra of ZnO NPs showed the excitonic absorption peaks at 222 nm in the presence of BMIMI while 227 nm in the absence of BMIMI. As for the absorption band, it was moved to the lowest wavelength and the blue shift of the quantum confinement effect indicating the production of ZnO NPs [86]. Another study that used $BMIMBF_4$ to synthesize the rare earth MONPs showed that by using UV-Vis spectrum data, the insertion of CeO_2 NPs into the chitosan polymer has a high ability of catalytic oxidative recovery. This can be confirmed by the spectrum shifting from lower to higher and higher to lower energy range with hydrogen peroxide aid. In addition, the valence states of cerium oxide (3^+ and 4^+) on the surface of nanoparticles fundamentally function as an antioxidant, which had been trapping free radicals in the culture medium that was validated using UV-Vis data [52] the sharp absorption band arise from the transition of valence band to conduction band of the MONPs. One can also notice that the absorption band of the maximum wavelength from the UV-vis spectra indicates that the RTILs affected structure formation of the particles as well as the optical properties of the synthesized MONPs. The absorption band showed a blue shift peak due to smaller particles size owing to the use of RTILs as capping agent in the synthesis of MONPs. However, there were studies that show a red shift region when they used RTILs in their synthesis due to the formation of mixed morphology (hexagonal, rectangular, and spherical) of the MONPs product or changing in the shape or structure of the particles such as from spherical to nanarod in the absence and presence of RTILs as a templating agent, respectively [110, 159].

Crystallinity analysis

X-ray powder diffraction

The XRD is a common technique used to study the crystal structures and atomic spacing based on the

constructive interference of monochromatic X-rays. A crystalline sample using XRD consist of three basic elements, namely an X-ray tube, a sample holder, and an X-ray detector [160, 161]. Moreover, XRD is suitable for various types of material such as fluids, metals, minerals, polymers, catalysts, plastics, pharmaceuticals, thin-film coatings, ceramics, solar cells, and semiconductors since it is a non-destructive method [160].

Also, XRD is a fingerprint technique used to study the crystallographic structures, purity, and atomic spacing of the MONPs, whether it is an amorphous or crystal structure based on the constructive interference of monochromatic X-rays and samples. The main distinctive peaks in XRD diffractograms that fit the experimental data of MONPs structure can be used to confirm the presence of MONPs [162, 163]. Meanwhile ZnO/CdO NPs rodlike particles were successfully synthesized by using the hydrothermal method in the ionic liquid medium (4-methylpyridine,2,2,2- trifluoroacetate) and can be clarified using XRD pattern after dried in air at 150 °C. The diffraction peaks were observed at 2θ = 34.0°, 35.0°, 37.05°, 48.04°, 57.03°, 68.02°, 69.00° correspond to (100), (002), (101), (102), (110), (112), and (201), respectively, these peaks are attributed to ZnO nanorod. Therefore, the as-synthesized products have great purity and crystallinity, as evidenced by the sharp and strong diffraction peaks from XRD pattern [163]. In addition to this, the synthesis of ZnO NPs with different pH by aqueous solution growth technique also successfully obtained ZnO NPs using Benzyltrimethylammoiumhydroxide (BTMAH) RTILs at different concentration and various pH. The micro/nanorods were extremely crystalline, as evidenced by XRD patterns with large, high-intensity peaks extending over the 2θ dimension. In this study, crystal planes were only reported at 100, 002, 101, 102, 110, 103, 200, 112, 201, 004 and 202. It was reported that due to the effect of ionic liquid concentration and pH the crystallite size was reduced with good crystallinity [165]. Similarly, Kowsari and Abdpour [166] also reported peaks at 2θ = 34.0, 35.0, 37.05, 48.04, 57.03, 63.04, 65.01, 68.02, 69.00 which corresponded to 100, 002, 101, 102, 110, 103, 200, 112, 201, respectively. The results show that the product is entirely made up of pure phase, with no impurity reflection peaks that indicates the hexagonal wurtzite structures of ZnO NPs when synthesis with functional RTILs, which are consistent with standard JCPDS: 792205 card ICSD#: 067454 [166]. From the reported journals, the synthesis of ZnO NPs using different type of RTILs as capping agents contribute to different crystal systems and a variety of MONPs structures as well as crystallite sizes.

Other than that, in the synthesis of TiO_2 N Ps using $BMIMBF_4$ was also investigated where the crystal plane was observed to be 101, 004, 200, 105, 204 indicated to anatase phase of the TiO_2 NPs without any trace of brookite and rutile phase detected. Based on this study there was a presence of brookite phase during the absence of the $BMIMBF_4$ where the XRD pattern showed a diffraction peak at 2θ=30.8º and disappeared when $BMIMBF_4$ were added amidst the synthesis of MONPs and a sharp diffraction appeared and increased at 2θ=25.4º with increasing amount of RTILs added [102]. A similar observation was also reported by Zheng et al. [32] who synthesis TiO_2 using different concentration EMIMBr and the XRD pattern showed a crystallite phase evolution of the synthesis TiO_2. The absence of EMIMBr gave about a 92% of anatase with minimal brookite phase in the system showing a crystal plane of 101, 004, 200, 105, and 211. The increasing of EMIMBr concentration led to growing of pure rutile phase in the crystal system with crystal plane of 110, 101, 200, 111, 210, 211, and 220. It is worth to noted that, different concentration of RTIL added into the reaction synthesis will provide diversity of crystal system. Therefore, researcher can utilize the amount of RTILs in order to obtain a desired crystal system of the TiO_2 NPs to make sure the suitability of the MONPs products for a curtained application.

Recent and future applications of MONPs synthesized in RTILs

The excellent properties of MONPs that are produced using RTILs as a capping agent were reported in many sectors including water treatment [30], super capacitance [33], catalyst [36], and antibacterial applications.

Antibacterial application

MONPs has drawn researchers interest due to their broad spectrum in antibacterial activities. New developments of antibacterial products or agents are in ominous need due to the resistance of microbial towards antibiotics through mutation process [167]. To investigate the antibacterial activity, the mechanism steps involved between MONPs and microbial are as follows [90, 167, 168, 169, 170, 171]. The MONPs adsorb on the surface of cell wall,

penetrating into the cell, therefore further modify the replication and respiration leading to cell death as reported previously

1. Promote the formation of reactive oxygen species (ROS) from the MONPs that can interact with proteins and/or intercalate between the purine and pyrimidine components that are present in DNA involving further damage in the cell membrane, and
2. Causing a cell death by disrupting the signal transduction pathways of the cells.

Muthulakshmi et al. [110], examined the uniform size of Yb_2O_3 NPs synthesized in the $BMIMPF_6$ as a capping agent during the formation of Yb_2O_3 NPs. The suitable concentrations Yb_2O_3 NPs (150 µg/mL) was added carefully on the plates containing gram positive of *S. aureus* and gram negative of *E. coli* which were cultured in the nutrient agar. After 24 hours, the inhibition zone of Yb_2O_3 NPs synthesized in $BMIMPF_6$ was found to be higher compared to Yb_2O_3 NPs synthesized without $BMIMPF_6$. On *E. coli*, the inhibition zones of Yb_2O_3 and RTIL-Yb_2O_3 NPs were 5 and 8 mm, respectively while the zone of inhibition of Yb_2O_3, RTILs-Yb_2O_3 NPs, on *S. aureus* was at 4 and 7 mm. The effectiveness of inhibition activities of Yb_2O_3 NPs due to formation of uniform size coverage on the bacterial systems, which allow metal cations to be released from MONPs to damage the cell wall by adhering to the bacteria's surface and interacting with cell wall amino acids [39]. A similar investigation has been performed by Sundarajan et al. [91], where $BMIMPF_6$ assisted Nd_2O_3 NPs acting as antibacterial agents pathogenic bacteria like *E. Coli* and *S. aureus*. Even at a very low concentration (10 µg/mL), Nd_2O_3 NPs assisted $BMIMPF_6$ to display a relevant zone of inhibitions indicateing a potential in bactericidal activity.

According to their finding, inhibition zone of gram-negative bacteria (*E. coli*) containing Nd_2O_3 NPs was found at 2 mm while double zone inhibitions were found at Nd_2O_3 NPs- $BMIMPF_6$ (4 mm). Similar observation was reported for the zone of inhibition of the Nd_2O_3 NPs (5 mm) against *Staphylococcus aureus* where the zone inhibition was found larger using Nd_2O_3- $BMIMPF_6$ (7 mm).

Likely, Sundrarajan et al. [86] examined an inhibition zone of ZnO NPs against gram negative of *E.coli* by different methods such as the zone of inhibition, growth curve and biofilm formation. In their finding, the improved morphologically material exhibited very good antibacterial activity against the gram-negative. The ZnO NPs (50 µg mL^{-1}) without RTILs after calcination produced maximum diameter of inhibition zone (2.2 cm) while a same concentration of ZnO NPs synthesized in BMIMI produced larger inhibition zones with a diameter of 3.2 cm, indicating stronger antibacterial activity. Furthermore, upon test on *E. coli* bacterium's biofilm architecture on glass, the control demonstrated biofilm bacterial strains' significant adhering capacity after incubation. However, confocal fluorescence micrograph revealed that ZnO NPs in BMIMI were more effective and active in reducing adhesion and biofilm formation, and that they inhibited bacterial growth better than ZnO NPs without BMIMI. These effective bactericidal capabilities could be attributed to the tiny particle size and enhanced shape of the synthesized material, which allowed for uniform distribution of Zn^{2+} ions on the bacterial surface, resulting in substantial antibacterial activity.

Another MONPs nanocomposite have been synthesis for biological activities has been studied by far to inhibit the growth of *Staphylococcus aureus* (Gram-positive) and *Escherichia coli* (Gram-negative) bacteria such as Ag-Au/Y_2O_3 NPs in $BMIMPF_6$ [93], Ag-Au doped RuO_2 NPs synthesized in $BMIMPF_6$ [151], silver/manganese oxide/bentonite nanocomposite synthesized in N-trimethyl-N-propylammonium bis(trifluoromethanesulfonyl) imide [91]. Different physiological features including shape, size, charge, and morphology have a significant impact on the antibacterial activity of MONPs aided RTILs. Small particles have a larger surface area than bulk material, allowing them to pass through the bacterial wall more quickly. MONPs with a smaller crystalline size are more effective at releasing ions and inhibiting bacterial growth by entering cell membranes and reacting with sulfhydryl inside the cell membranes. As a result, the MONPs break the membrane and render proteins inactive, causing the bacterial cell to die [94].

Catalyst

Researchers are interested in developing photocatalysts with a mesoporous shape to produce high photocatalytic activity and promote quick intraparticle molecular transfer. To acquire higher photocatalyst characteristics, bigger surface area particles are necessary to improve light harvesting and adsorption for reactant molecules. For example, Liu et

al., [102] described the synthesis of TiO_2 NPs in $BMIMBF_4$ where the addition of $BMIMBF_4$ encouraged the formation of anatase TiO_2 NPs. The material was very thermally stable which enabled the preservation of anatase phase even after calcination at 900 °C. The photocatalytic activity of TiO_2 prepared with $BMIMBF_4$ was higher than that of the sample prepared without RTILs attributed to a larger surface area, good anatase crystal mesostructured and small particles size of synthesized material.

Subsequently, Liu et al. [147] investigated the photocatalytic activity of CeO_2–TiO_2 NPs produced in $C_{16}MIMBr$ for the degradation of p-chlorophenol aqueous solution under UV and visible-light irradiation using well-crystallized CeO_2–TiO_2 NPs. During the research, they discovered that 10% CeO_2–TiO_2 NPs had the maximum photoactivity under UV and visible light irradiation, with degradation rates of 95.3% and 57.5%, respectively. This activity was supported by the greater surface area, higher Ce^{3+} concentration, highest surface hydroxyl group concentration, and strongest light absorbance due to the smaller particle size (11–16 nm) formed in the synthesis. Meanwhile, Kayva et al. [36] reported the use of ZnO NPs synthesized in $OMIMPF_6$ (capping agent) to reduce the agglomeration via microwave irradiation method in esterification. Due to its good reproducibility, ZnO NPs as the smart material acts as a solid acid catalyst in the esterification process as it can be used up to four cycles. The authors discovered that the catalysts managed to enhance the percentage yield of primary alcohol to almost 80%.

Other applications

According to Atta et al., ZnO NPs are environmentally friendly nanocomposites for water treatment applications due to their antimicrobial and superior properties. In their work, poly-IL (PIL) based quaternary ammonium salts of 2–acrylamido-2-methyl propane sulfonic acid homopolymer and its copolymer, N-vinyl pyrrolidone, were used as capping agents to control the shapes and sizes of ZnO NPs. The prepared ZnO NPs were successfully crosslinked to 2–acrylamido-2-methyl propane sulfonic acid-co-acrylonitrile nanocomposites, which were used as adsorbents for methylene blue dye, as one of the efforts to reduce a hazardous organic pollutant found in water. The enhanced properties of ZnO NPs showed high removal rates than that used without ZnO NPs [30]. Bharate et al. [33] synthesized MnO_2 NPs in IL for supercapacitor application as an electrode material. The study revealed that MnO_2 NPs displayed different morphology in the presence of nanorod-shaped RTILs and the absence of spherical-shaped RTILs. As for the supercapacitor study, cyclic voltammetry and charge-discharge analysis were performed using an electrode modified with MnO_2-capped RTILs. The electrode generated substantial pseudo-capacitance reaching a maximum value probably due to the supercapacitor assembled with RTILs capped MnO_2 NPs, as positive and negative electrodes, resulting in high specific capacitance and better rate capability. Based on the available literature, remarkably excellent properties have been reported in studies of MONPs synthesized in RTILs in various fields. Therefore, the synthesis of other materials could be now investigated in the RTILs to obtain improved physiological properties.

Conclusion

In conclusion, he synthesis of MONPs commonly involve chemical methods which include sol-gel, hydrothermal, ultrasound-assisted, precipitation, and microwave-assisted. This paper provided a comprehensive review of the common techniques of preparation and characterization of MONPs using RTILs. In general, the MONPs could be prepared using various RTILs by chemical method followed by calcination and characterization to get the desired structure and morphology of the MONPs. SEM/EDX and TEM were used to study the structure and morphology of the synthesized MONPs, whereas XRD was used to study the crystallinity and purity of the synthesized MONPs. Meanwhile, FTIR and UV-VIS were used to study the shifting of the functional group of the MONPs and the maximum wavelength shifting of absorbance of the synthesis MONPs. Based on the studies, various structure and morphology of the MONPs have been reported and can be tailor-made using different RTILs for the synthesis of specific MONPs. On the other hand, the impacts of RTILs on the formation of MONPs which reduces the agglomeration during the growth steps was also extensively discussed in this review. Moreover, this review recapitulated the applications of MONPs synthesized using RTILs with enhanced properties in antibacterial, catalyst, and other applications. For example, in antibacterial application, the inhibition zone of bacteria for MONPs that were synthesized using RTILs were doubled rather than the MONPs that were not synthesized using RTILs. In short, this review would be beneficial for manufacturers custom-made materials of MONPs using RTILs with effective properties. Finally, it is hoped that this review will not

only exhibit the recent progress in the synthesis of MONPs using RTILs, but also embark further research to explore insightful and green methods for the preparation of MONPs.

Acknowledgement

The authors gratefully acknowledge the financial support by Ministry of Education Malaysia (Fundamental Research Grant Scheme FRGS/1/ 2019/STG05/UITM/03/3). The authors acknowledge Faculty of Applied Science UiTM Shah Alam and Centre for Research and Instrumentation Management (CRIM) for the analytical services given.

References

1. Thanh, N. T. K., Maclean, N. and Mahiddine, S. (2014). Mechanisms of nucleation and growth of nanoparticles in solution. *Chemical Reviews*, 114(15): 7610-7630.
2. He, Z. and Alexandridis, P. (2017). Ionic liquid and nanoparticle hybrid systems: Emerging applications. *Advances in Colloid and Interface Science*, 244: 54-70.
3. McNamara, K. and Tofail, S. A. M. (2017). Nanoparticles in biomedical applications. *Advances in Physics: X*, *2*(1): 54-88.
4. Nikolova, M. P. and Chavali, M. S. (2020). Metal oxide nanoparticles as biomedical materials. *Biomimetics*, 5(2): 27.
5. Stankic, S., Suman, S., Haque, F. and Vidic, J. (2016). Pure and multi metal oxide nanoparticles: Synthesis, antibacterial and cytotoxic properties. *Journal of Nanobiotechnology*, 14(1): 1-20.
6. Andreescu, S., Ornatska, M., Erlichman, J. S., Ana, E. and Leiter, J. C. (2011). Biomedical applications of metal oxide nanoparticles. In *Fine Particles in Medicine and Pharmacy*. (Egon Matijević Editor). Springerlink Book: pp. 57-100.
7. Joshi, M. and Roy, A. (2018). Antimicrobial textiles based on metal and metal oxide nano-particles. *Nanomaterials in the Wet Processing of Textiles*, 2018: 71-111.
8. Raghunath, A. and Perumal, E. (2017). Metal oxide nanoparticles as antimicrobial agents: a promise for the future. *International Journal of Antimicrobial Agents*, 49(2): 137-152.
9. Nagajyothi, P. C., Prabhakar Vattikuti, S. V., Devarayapalli, K. C., Yoo, K., Shim, J. and Sreekanth, T. V. M. (2020). Green synthesis: Photocatalytic degradation of textile dyes using metal and metal oxide nanoparticles-latest trends and advancements. *Critical Reviews in Environmental Science and Technology*, 50(24): 2617-2723.
10. Khan, M. M., Adil, S. F. and Al-Mayouf, A. (2015). Metal oxides as photocatalysts. *Journal of Saudi Chemical Society*, 19(5): 462-464.
11. Veerasingam, M., Murugesan, B. and Mahalingam, S. (2020). Ionic liquid mediated morphologically improved lanthanum oxide nanoparticles by Andrographis paniculata leaves extract and its biomedical applications. *Journal of Rare Earths*, 38(3): 281-291.
12. Cheng, Z., Tan, A. L. K., Tao, Y., Shan, D., Ting, K. E. and Yin, X. J. (2012). Synthesis and characterization of iron oxide nanoparticles and applications in the removal of heavy metals from industrial wastewater. *International Journal of Photoenergy*, 2012: 608298.
13. Zhu, D., Chen, Y., Yang, H., Wang, S., Wang, X., Zhang, S. and Chen, H. (2020). Synthesis and characterization of magnesium oxide nanoparticle-containing biochar composites for efficient phosphorus removal from aqueous solution. *Chemosphere*, 247: 125847.
14. Dang, T. D., Cheney, M. A., Qian, S., Joo, S. W. and Min, B. K. (2013). A novel rapid one-step synthesis of manganese oxide nanoparticles at room temperature using poly(dimethylsiloxane). *Industrial and Engineering Chemistry Research*, 52(7): 2750-2753.
15. Dawadi, S., Gupta, A., Khatri, M., Budhathoki, B., Lamichhane, G. and Parajuli, N. (2020). Manganese dioxide nanoparticles: synthesis, application and challenges. *Bulletin of Materials Science*, 43: 227.
16. Mahamuni, P. P., Patil, P. M., Dhanavade, M. J., Badiger, M. V., Shadija, P. G., Lokhande, A. C. and Bohara, R. A. (2019). Synthesis and characterization of zinc oxide nanoparticles by using polyol chemistry for their antimicrobial and antibiofilm activity. *Biochemistry and Biophysics Reports*, 17(9): 71-80.
17. Elbushra, H., Ahmed, M., Wardi, H. and Eassa, N. (2018). Synthesis and characterization of TiO_2 using sol-gel method at different annealing temperatures. *MRS Advances*, 3(42–43): 2527-2535.
18. Singh, P. K., Kumar, P., Hussain, M., Das, A. K. and Nayak, G. C. (2016). Synthesis and characterization of CuO nanoparticles using strong base electrolyte through electrochemical discharge process. *Bulletin of Materials Science*, 39(2): 469-478.

19. Fathima, J. B., Pugazhendhi, A. and Venis, R. (2017). Synthesis and characterization of ZrO_2 nanoparticles-antimicrobial activity and their prospective role in dental care. *Microbial Pathogenesis*, 110: 245-251.
20. Dubey, R. S., Rajesh, Y. B. R. D. and More, M. A. (2015). Synthesis and Characterization of SiO_2 nanoparticles via sol-gel method for industrial applications. *Materials Today: Proceedings*, 2(4–5): 3575-3579.
21. Sakthiraj, K. and Karthikeyan, B. (2020). Synthesis and characterization of cerium oxide nanoparticles using different solvents for electrochemical applications. *Applied Physics A: Materials Science and Processing*, 126(1): 1-10.
22. Wang, C., Xu, H., Wang, C., Liu, T., Yang, S., Nie, Y., Guo, X., Ma, X. and Jiang, X. (2021). Preparation of VO2 (M) nanoparticles with exemplary optical performance from VO2 (B) nanobelts by ball milling. *Journal of Alloys and Compounds*, 877: 159888.
23. Malevu, T. D. (2021). Ball Milling synthesis and characterization of highly crystalline TiO_2-ZnO hybrids for photovoltaic applications . *Physica B: Condensed Matter*, 621(7): 413291.
24. Rashid, T. M., Nayef, U. M., Jabir, M. S., and Mutlak, F. A. H. (2021). Synthesis and characterization of Au:ZnO (core:shell) nanoparticles via laser ablation. *Optik*, 244(7): 167569.
25. Altuwirqi, R. M., Albakri, A. S., Al-Jawhari, H. and Ganash, E. A. (2020). Green synthesis of copper oxide nanoparticles by pulsed laser ablation in spinach leaves extract. *Optik*, 219(4): 165280.
26. Menazea, A. A. and Awwad, N. S. (2020). Pulsed Nd:YAG laser deposition-assisted synthesis of silver/copper oxide nanocomposite thin film for 4-nitrophenol reduction. *Radiation Physics and Chemistry*, 177(5): 109112.
27. Shreema, K., Mathammal, R., Kalaiselvi, V., Vijayakumar, S., Selvakumar, K. and Senthil, K. (2021). Green synthesis of silver doped zinc oxide nanoparticles using fresh leaf extract *Morinda citrifoliaand* its antioxidant potential. *Materials Today: Proceedings*, 47: 2126-2131.
28. Ramzan, M., Obodo, R. M., Mukhtar, S., Ilyas, S. Z., Aziz, F. and Thovhogi, N. (2019). Green synthesis of copper oxide nanoparticles using Cedrus deodara aqueous extract for antibacterial activity. *Materials Today: Proceedings*, 36: 576-581.
29. Khan, M. F., Ansari, A. H., Hameedullah, M., Ahmad, E., Husain, F. M., Zia, Q., Baig, U., Zaheer, M. R., Alam, M. M., Khan, A. M., Alothman, Z. A., Ahmad, I., Ashraf, G. M. and Aliev, G. (2016). Sol-gel synthesis of thorn-like ZnO nanoparticles endorsing mechanical stirring effect and their antimicrobial activities: Potential role as nano-Antibiotics. *Scientific Reports*, 6(5): 1-12.
30. Atta, A. M., Al-Lohedan, H. A., Ezzat, A. O., Tawfik, A. M. and Hashem, A. I. (2017). Synthesis of zinc oxide nanocomposites using poly (ionic liquids) based on quaternary ammonium acrylamidomethyl propane sulfonate for water treatment. *Journal of Molecular Liquids*, 236: 38-47.
31. Wang, Y., Maksimuk, S., Shen, R. and Yang, H. (2007). Synthesis of iron oxide nanoparticles using a freshly-made or recycled imidazolium-based ionic liquid. *Green Chemistry,* 10: 1051-1056.
32. Zheng, W., Liu, X., Yan, Z. and Zhu, L. (2009). Ionic liquid-assisted synthesis of large-scale TiO_2 nanoparticles with controllable phase by hydrolysis of TiCl4. *ACS Nano*, *3*(1): 115-122.
33. Bharate, B. G., Hande, P. E., Samui, A. B. and Kulkarni, P. S. (2018). Ionic liquid (IL) capped MnO_2 nanoparticles as an electrode material and IL as electrolyte for supercapacitor application. *Renewable Energy,* 126: 437-444.
34. Sivanantham, A., Firoz Babu, K., Anbu Kulandainathan, M., Babu, S. G., Suresh Bapu, R. H. and Sreedhar, G. (2014). Capping and catalytic behaviour of lithiated sarcosine TFSI on the formation of hexagonal ZnO micro rods using hydrothermal method. *Materials Letters*, 128: 195-198.
35. Qi, K., Yang, J., Fu, J., Wang, G., Zhu, L., Liu, G. and Zheng, W. (2013). Morphology-controllable ZnO rings: Ionic liquid-assisted hydrothermal synthesis, growth mechanism and photoluminescence properties. *CrystEngComm*, 15(34): 6729-6735.
36. Kavya, S. H., Kumar, V. V., & Kumar, C. R. (2018). Synthesis and characterization of stable ZnO nanoparticles using imidazolium-based ionic liquids and their applications in esterification reaction. *Indian Journal of Chemistry, 57*: 1112-1120.
37. Ahmadi Tehrani, A., Omranpoor, M. M., Vatanara, A., Seyedabadi, M. and Ramezani, V. (2019). Formation of nanosuspensions in bottom-

up approach: theories and optimization. *DARU Journal of Pharmaceutical Sciences*, 27(1): 451-473.

38. Jalab, J., Abdelwahed, W., Kitaz, A. and Al-kayali, R. (2021). Green synthesis of silver nanoparticles using aqueous extract of Acacia cyanophylla and its antibacterial activity. *Heliyon, 7*(9): e08033.
39. Khan, M. A. R., Shamim, M., Mamun, A. and Hosna, M. (2021). Review on platinum nanoparticles : Synthesis , characterization , and applications. *Microchemical Journal*, 171(9): 106840.
40. Devatha, C. P. and Thalla, A. K. (2018). Chapter 7 - green synthesis of nanomaterials (pp. 169-184). Elsevier.
41. Alam, M. M., Asiri, A. M. and Rahman, M. M. (2021). Wet-chemically synthesis of SnO_2-doped Ag_2O nanostructured materials for sensitive detection of choline by an alternative electrochemical approach. *Microchemical Journal*, 165(2): 106092.
42. Nikam, A. V., Prasad, B. L. V. and Kulkarni, A. A. (2018). Wet chemical synthesis of metal oxide nanoparticles: A review. *CrystEngComm*, 20(35): 5091-5107.
43. Zhou, Y. (2006). Recent advances in ionic liquids for synthesis of inorganic nanomaterials. *Current Nanoscience*, 1(1): 35-42.
44. Irfan, M., Ahmad, T., Moniruzzaman, M., Bhattacharjee, S. and Abdullah, B. (2020). Size and stability modulation of ionic liquid functionalized gold nanoparticles synthesized using *Elaeis guineensis* (oil palm) kernel extract. *Arabian Journal of Chemistry*, 13(1): 75-85.
45. Nishad, K K., Manthrammel, M. A., Shkir, M., AlFaify, S. and Pandey, R. K. (2022). Effect of organic capping on defect induced ferromagnetism in ZnO nanoparticles. *Physica B: Condensed Matter*, 624: 413379.
46. Rostami-Tapeh-Esmaeil, E., Golshan, M., Salami-Kalajahi, M. and Roghani-Mamaqani, H. (2021). Synthesis of copper and copper oxide nanoparticles with different morphologies using aniline as reducing agent. *Solid State Communications*, 334-335(5): 114364.
47. Yong, N. L., Ahmad, A., & Mohammad, A. W. (2012). Synthesis and characterization of silver nanoparticles by a sonochemical method. *Xiyou Jinshu Cailiao Yu Gongcheng/Rare Metal Materials and Engineering*, 41(10): 1700-1705.
48. Saraji, M. and Alijani, S. (2021). A molecularly imprinted polymer on chromium (III) oxide nanoparticles for spectrofluorometric detection of bisphenol A. *Spectrochimica Acta - Part A: Molecular and Biomolecular Spectroscopy*, 255: 119711.
49. Sedlák, J., Kuřitka, I., Machovský, M., Šuly, P., Bažant, P. and Sedláček, T. (2015). Zinc oxide nanoparticles with surface modified by degradation of capping polymers in situ during microwave synthesis. *Advanced Powder Technology*, 26(4): 1064-1071.
50. Bomila, R., Venkatesan, A. and Srinivasan, S. (2018). Structural, luminescence and photocatalytic properties of pure and octylamine capped ZnO nanoparticles. *Optik*, 158: 565-573.
51. Hajipour, A. R. and Rafiee, F. (2015). Recent progress in ionic liquids and their applications in organic synthesis. *Organic Preparations and Procedures International*, 47(4): 1-60.
52. Fang, X. and Song, H. (2019). Synthesis of cerium oxide nanoparticles loaded on chitosan for enhanced auto-catalytic regenerative ability and biocompatibility for the spinal cord injury repair. *Journal of Photochemistry and Photobiology B: Biology*, 191: 83-87.
53. Sundrarajan, M., Jegatheeswaran, S., Selvam, S., Sanjeevi, N. and Balaji, M. (2015). The ionic liquid assisted green synthesis of hydroxyapatite nanoplates by *Moringa oleifera* flower extract: A biomimetic approach. *Materials and Design*, *88*: 1183-1190.
54. Łuczak, J., Paszkiewicz, M., Krukowska, A., Malankowska, A. and Zaleska-Medynska, A. (2016). Ionic liquids for nano- and microstructures preparation. Part 2: Application in synthesis. *Advances in Colloid and Interface Science*, 227: 1-52.
55. Migowski, P., Machado, G., Texeira, S. R., Alves, M. C. M., Morais, J., Traverse, A. and Dupont, J. (2007). Synthesis and characterization of nickel nanoparticles dispersed in imidazolium ionic liquids. *Physical Chemistry Chemical Physics*, 9(34): 4814-4821.
56. Vollmer, C. and Janiak, C. (2011). Naked metal nanoparticles from metal carbonyls in ionic liquids: Easy synthesis and stabilization. *Coordination Chemistry Reviews*, *255*(17-18): 2039-2057.
57. Scheeren, C. W., Machado, G., Teixeira, S. R., Morais, J., Domingos, J. B. and Dupont, J. (2006). Synthesis and characterization of Pt(0) nanoparticles in imidazolium ionic liquids.

Journal of Physical Chemistry B, 110(26): 13011-13020.

58. Zhao, M., Li, N., Zheng, L., Li, G. and Yu, L. (2008). Synthesis of well-dispersed NiO nanoparticles with a room temperature ionic liquid. *Journal of Dispersion Science and Technology,* 29(8): 1103-1105.
59. Sakai, K., Okada, K., Uka, A., Misono, T., Endo, T., Sasaki, S., Abe, M. and Sakai, H. (2015). Effects of water on solvation layers of imidazolium-type room temperature ionic liquids on silica and mica. *Langmuir*, 31(22), 6085–6091.
60. Ninham, B. W. (1999). On progress in forces since the DLVO theory. *Advances in Colloid and Interface Science*, 83(1): 1-17.
61. Obliosca, J. M., Arellano, I. H. J., Huang, M. H. and Arco, S. D. (2010). Double layer micellar stabilization of gold nanocrystals by greener ionic liquid 1-butyl-3-methylimidazolium lauryl sulfate. *Materials Letters*, 64(9): 1109-1112.
62. He, Z., & Alexandridis, P. (2015). Nanoparticles in ionic liquids: Interactions and organization. *Physical Chemistry Chemical Physics*, 17(28): 18238-18261.
63. Barik, B., Kumar, A., Nayak, P. S., Achary, L. S. K., Rout, L. and Dash, P. (2020). Ionic liquid assisted mesoporous silica-graphene oxide nanocomposite synthesis and its application for removal of heavy metal ions from water. *Materials Chemistry and Physics*, 239(8): 122028.
64. Das, M., Aswathy, T. R., Pal, S. and Naskar, K. (2021). Effect of ionic liquid modified graphene oxide on mechanical and self-healing application of an ionic elastomer. *European Polymer Journal*, 158(7): 110691.
65. Kargar, S., Elhamifar, D. and Zarnegaryan, A. (2021). Ionic liquid modified graphene oxide supported Mo-complex: A novel, efficient and highly stable catalyst. *Surfaces and Interfaces*, 23(1): 100946.
66. Husanu, E., Chiappe, C., Bernardini, A., Cappello, V. and Gemmi, M. (2018). Synthesis of colloidal Ag nanoparticles with citrate based ionic liquids as reducing and capping agents. *Colloids and Surfaces A: Physicochemical and Engineering Aspects*, 538(11): 506-512.
67. Sadeghi, S. and Olieaei, S. (2019). Capped cadmium sulfide quantum dots with a new ionic liquid as a fluorescent probe for sensitive detection of florfenicol in meat samples. *Spectrochimica Acta - Part A: Molecular and Biomolecular Spectroscopy*, 223: 117349.
68. Krishnan, B. and Mahalingam, S. (2017). Improved surface morphology of silver/copper oxide/bentonite nanocomposite using aliphatic ammonium based ionic liquid for enhanced biological activities. *Journal of Molecular Liquids*, 241: 1044-1058.
69. Ahmad, T., Bustam, M. A., Irfan, M., Moniruzzaman, M., Samsudin, M. F. R., Asghar, H. M. A., Muhammad, N., Iqbal, J. and Bhattacharjee, S. (2019). Effect of gold and iron nanoparticles on photocatalytic behaviour of titanium dioxide towards 1-butyl-3-methylimidazolium chloride ionic liquid. *Journal of Molecular Liquids*, 291: 2–6.
70. Verma, C., Ebenso, E. E. and Quraishi, M. A. (2019). Transition metal nanoparticles in ionic liquids: Synthesis and stabilization. *Journal of Molecular Liquids*, 276: 826-849.
71. Abbott, A. P., Frisch, G., Hartley, J. and Ryder, K. S. (2011). Processing of metals and metal oxides using ionic liquids. *Green Chemistry*, 13(3): 471-481.
72. Prechtl, M. H. G. and Campbell, P. S. (2013). Metal oxide and bimetallic nanoparticles in ionic liquids: Synthesis and application in multiphase catalysis. *Nanotechnology Reviews*, 2(5): 577-595.
73. Seitkalieva, M. M., Samoylenko, D. E., Lotsman, K. A., Rodygin, K. S. and Ananikov, V. P. (2021). Metal nanoparticles in ionic liquids: Synthesis and catalytic applications. *Coordination Chemistry Reviews*, 445: 213982.
74. Gulati, S., Sachdeva, M. and Bhasin, K. K. (2018). Capping agents in nanoparticle synthesis: Surfactant and solvent system. *AIP Conference Proceedings*, 2018: 1953.
75. Tapak, N. S., Nawawi, M. A., Tjih, E. T. T., Mohd, Y., Ab Rashid, A. H., Abdullah, J., ... and Ahmad, N. M. (2022). The synthesis of zirconium oxide (ZrO2) nanoparticles (NPs) in 1-butyl-3-methylimidazolium trifluoroacetate (BMIM CF_3COO) for an amperometry phenol biosensor. *Materials Today Communications,* 33: 104142.
76. Oskam, G. (2006). Metal oxide nanoparticles: Synthesis, characterization and application. *Journal of Sol-Gel Science and Technology*, 37(3): 161-164.
77. Hu, H., Huang, X., Deng, C., Chen, X. and Qian, Y. (2007). Hydrothermal synthesis of ZnO nanowires and nanobelts on a large scale. *Materials Chemistry and Physics*, 106(1): 58-62.

78. Zhang, S., Zhang, Y., Wang, Y., Liu, S. and Deng, Y. (2012). Sonochemical formation of iron oxide nanoparticles in ionic liquids for magnetic liquid marble. *Physical Chemical Chemistry Physics,* 15: 5132-5138.
79. Janiak, C. (2013). Ionic liquids for the synthesis and stabilization of metal nanoparticles. Zeitschrift Fur Naturforschung - Section B Journal of Chemical Sciences, 68(10): 1059-1089
80. Alammar, T. and Mudring, A. V. (2011). Sonochemical synthesis of 0D, 1D, and 2D zinc oxide nanostructures in ionic liquids and their photocatalytic activity. *ChemSusChem*, 4(12): 1796-1804.
81. Wang, L., Chang, L., Zhao, B., Yuan, Z., Shao, G. and Zheng, W. (2008). Systematic investigation on morphologies, forming mechanism, photocatalytic and photoluminescent properties of ZnO nanostructures constructed in ionic liquids. *Inorganic Chemistry*, 47(5): 1443-1452.
82. Zhu, H., Huang, J. F., Pan, Z. and Dai, S. (2006). Ionothermal synthesis of hierarchical ZnO nanostructures from ionic-liquid precursors. *Chemistry of Materials*, 18(18): 4473-4477.
83. Ma, B. Z., Yu, J. and Dai, S. (2010). Preparation of inorganic materials using ionic liquids. *Advance Materials,* 130012: 261-285.
84. Lian, J., Duan, X., Ma, J., Peng, P., Kim, T., & Zheng, W. (2009). Hematite (α-Fe_2O_3) with various morphologies: ionic liquid-assisted synthesis, formation mechanism, and properties. *ACS Nano, 3*(11): 3749-3761.
85. Zhang, Y., Cheng, X., Zhang, X., Major, Z., Xu, Y., Gao, S., Zhao, H. and Huo, L. (2019). Ionic liquid-assisted synthesis of tungsten oxide nanoparticles with enhanced NO_2 sensing properties at near room temperature. *Applied Surface Science*, 2: 144533.
86. Sundrarajan, M., Jegatheeswaran, S., Selvam, S., Gowri, R., Balaji, M. and Bharathi, K. (2017). Green approach : Ionic liquid assisted synthesis of nanocrystalline ZnO in phyto medium and their antibacterial investigation. *Materials Letters*, 201: 31-34.
87. Fang, X. and Song, H. (2019). Synthesis of cerium oxide nanoparticles loaded on chitosan for enhanced auto-catalytic regenerative ability and biocompatibility for the spinal cord injury repair. *Journal of Photochemistry and Photobiology B: Biology*, 191: 83-87.
88. Sundrarajan, M., Gandhi, R. G. R., Suresh, J., Selvam, S. and Gowri, S. (2012). Sol-gel synthesis of MgO nanoparticles using ionic liquid-[BMIM]BF_4 as capping agent. *Nanoscience and Nanotechnology Letters*, 4(1): 100-104.
89. Yoo, K., Choi, H. and Dionysiou, D. D. (2004). Ionic liquid assisted preparation of nanostructured TiO_2 particles. Chemical Communications, 17: 2000-2001.
90. García Rojas, L. M., Huerta-Aguilar, C. A., Tecuapa-Flores, E. D., Huerta-José, D. S., Thangarasu, P., Sidhu, J. S., Singh, N. and de la Luz Corea Téllez, M. (2020). Why ionic liquids coated ZnO nanocomposites emerging as environmental remediates: Enhanced photo-oxidation of 4-nitroaniline and encouraged antibacterial behavior. *Journal of Molecular Liquids*, 319: 114107.
91. Sundrarajan, M. and Muthulakshmi, V. (2021). Green synthesis of ionic liquid mediated neodymium oxide nanoparticles by Andrographis paniculata leaves extract for effective bio-medical applications. *Journal of Environmental Chemical Engineering*, *9*(1): 104716.
92. Sundrarajan, M., Bama, K., Selvanathan, G. and Prabhu, M. R. (2018). Ionic liquid-mediated: Enhanced surface morphology of silver/manganese oxide/bentonite nanocomposite for improved biological activities. *Journal of Molecular Liquids*, 249: 1020-1032.
93. Pandiyan, N., Murugesan, B., Sonamuthu, J., Samayanan, S. and Mahalingam, S. (2019). [BMIM]PF_6 ionic liquid mediated green synthesis of ceramic SrO/CeO_2 nanostructure using *Pedalium murex* leaf extract and their antioxidant and antibacterial activities. *Ceramics International*, 45(9): 12138-12148.
94. Pandiyan, N., Murugesan, B., Arumugam, M., Chinnaalagu, D., Samayanan, S. and Mahalingam, S. (2021). Ionic liquid mediated green synthesis of Ag-Au/Y_2O_3 nanoparticles using leaves extracts of Justicia adhatoda: Structural characterization and its biological applications. *Advanced Powder Technology*, 32(7): 2213-2225.
95. Muthulakshmi, V. and Sundrarajan, M. (2020). Green synthesis of ionic liquid assisted ytterbium oxide nanoparticles by Couroupita guianensis abul leaves extract for biological applications. *Journal of Environmental Chemical Engineering*, 8(4): 103992.
96. Shen, J., Shi, M., Yan, B., Ma, H., Li, N. and Ye, M. (2011). One-pot hydrothermal synthesis of

Ag-reduced graphene oxide composite with ionic liquid. *Journal of Materials Chemistry,* 21(21): 7795-7801.

97. Lv, J. J., Feng, J. X., Li, S. S., Wang, Y. Y., Wang, A. J., Zhang, Q. L., Chen, J. R. and Feng, J. J. (2014). Ionic liquid crystal-assisted synthesis of PtAg nanoflowers on reduced graphene oxide and their enhanced electrocatalytic activity toward oxygen reduction reaction. *Electrochimica Acta*, 133: 407-413.
98. Zhang, J., Wang, J., Zhou, S., Duan, K., Feng, B., Weng, J., Tang, H. and Wu, P. (2010). Ionic liquid-controlled synthesis of ZnO microspheres. *Journal of Materials Chemistry*, 20(43): 9798-9804.
99. Kim, T., Lian, J., Ma, J., Duan, X. and Zheng, W. (2010). Morphology controllable synthesis of γ-alumina nanostructures via an ionic liquid-assisted hydrothermal route. *Crystal Growth and Design*, 10(7): 292-2933.
100. Muthulakshmi, V., Balaji, M. and Sundrarajan, M. (2020). Biomedical applications of ionic liquid mediated samarium oxide nanoparticles by *Andrographis paniculata* leaves extract. *Materials Chemistry and Physics*, 242(11): 122483.
101. Liu, H., Wang, M., Wang, Y., Liang, Y., Cao, W. and Su, Y. (2011). Ionic liquid-templated synthesis of mesoporous CeO_2–TiO_2 nanoparticles and their enhanced photocatalytic activities under UV or visible light. *Journal of Photochemistry & Photobiology, A: Chemistry, 223*(2–3): 157-164.
102. Liu, H., Liang, Y., Hu, H. and Wang, M. (2009). Hydrothermal synthesis of mesostructured nanocrystalline TiO 2 in an ionic liquid – water mixture and its photocatalytic performance. *Solid State Sciences*, 11(9): 1655-1660.
103. Gao, R., Gao, S., Wang, P., Xu, Y., Zhang, X., Cheng, X., Zhou, X., Major, Z., Zhu, H. and Huo, L. (2020). Ionic liquid assisted synthesis of snowflake ZnO for detection of NOx and sensing mechanism. *Sensors and Actuators, B: Chemical*, 303: 127085.
104. Goharshadi, E. K., Ding, Y., Namayandeh, M. and Nancarrow, P. (2009). Ultrasound-assisted green synthesis of nanocrystalline ZnO in the ionic liquid [hmim][NTf_2]. *Ultrasonics Sonochemistry*, 16: 120-123.
105. Inbasekar, C. and Fathima, N. N. (2020). Collagen stabilization using ionic liquid functionalised cerium oxide nanoparticle. *International Journal of Biological Macromolecules*, 147: 24-28.
106. Ellateif, T. M. A. and Mitra, S. (2017). Sol gel synthesis and characterization of zirconia containing hydrophobic silica nanoparticles. *Journal of Advances in Nanomaterials*, *2*(4): 185-196.
107. Lu, Y., Dong, W., Ding, J., Wang, W. and Wang, A. (2019). Hydroxyapatite nanomaterials: synthesis, properties, and functional applications. In *Nanomaterials from Clay Minerals*. Elsevier Inc.
108. Lim, H. S., Ahmad, A. and Hamzah, H. (2013). Synthesis of zirconium oxide nanoparticle by sol-gel technique. *AIP Conference Proceedings*, 1571: 812–816.
109. Behbahani, A., Rowshanzamir, S. and Esmaeilifar, A. (2012). Hydrothermal synthesis of zirconia nanoparticles from commercial zirconia. *Procedia Engineering*, 42: 908-917.
110. Muthulakshmi, V., Kumar, P. and Sundrarajan, M. (2021). Green synthesis of Ionic liquid mediated Ytterbium oxide nanoparticles by *Andrographis paniculata* leaves extract for structural, morphological and biomedical applications. *Journal of Environmental Chemical Engineering*, 9(4): 105270.
111. Jolivet, J. P., Cassaignon, S., Chanéac, C., Chiche, D., Durupthy, O. and Portehault, D. (2010). Design of metal oxide nanoparticles: Control of size, shape, crystalline structure and functionalization by aqueous chemistry. *Comptes Rendus Chimie*, 13(1–2): 40-51.
112. Kotresh, M. G., Patil, M. K. and Inamdar, S. R. (2021). Reaction temperature based synthesis of ZnO nanoparticles using co-precipitation method: Detailed structural and optical characterization. *Optik*, 243(6): 167506.
113. Wahab, R., Kim, Y. S. and Shin, H. S. (2009). Synthesis, characterization and effect of pH variation on zinc oxide nanostructures. *Materials Transactions*, 50(8): 2092-2097.
114. Nair, P. A. K., Vasconcelos, W. L., Paine, K. and Calabria-Holley, J. (2021). A review on applications of sol-gel science in cement. *Construction and Building Materials*, 291: 123065.
115. Danks, A. E., Hall, S. R. and Schnepp, Z. (2016). The evolution of 'sol–gel' chemistry as a technique for materials synthesis. *Materials Horizon,* 2: 91-112.
116. Shandilya, M., Rai, R., Singh, J., Shandilya, M.,

Rai, R. and Singh, J. (2016). Review: hydrothermal technology for smart materials. *Advances in Applied Chemistry,* 115: 354-376.

117. Sahoo, S., Pazhamalai, P., Mariappan, V. K., Veerasubramani, G. K., Nam-Jin Kim, Kim, S.-J. and A. (2020). Hydrothermally synthesized chalcopyrite platelets as electrode material for symmetric supercapacitors. *Inorganic Chemistry Frontiers*, 2020: 1-30.
118. Yadav, S. and Sharma, A. (2021). Importance and challenges of hydrothermal technique for synthesis of transition metal oxides and composites as supercapacitor electrode materials. *Journal of Energy Storage*, 44: 103295.
119. Ng, H. K. M., Lim, G. K. and Leo, C. P. (2021). Comparison between hydrothermal and microwave-assisted synthesis of carbon dots from biowaste and chemical for heavy metal detection : A review. *Microchemical Journal*, 165: 106116.
120. Medeiros, T. V. de, Manioudakis, J., Noun, F., Macairan, J.-R., Victoria, F. and Naccache, R. (2019). Microwave-assisted synthesis of carbon dots and their applications. *Materials Chemistry C*, 2019: 1-20.
121. Jusuf, B. N., Sambudi, N. S., Isnaeni, I. and Samsuri, S. (2018). Microwave-assisted synthesis of carbon dots from eggshell membrane ashes by using sodium hydroxide and their usage for degradation of methylene blue. *Journal of Environmental Chemical Engineering*, 6(6): 7426-7433.
122. Wang, X., Ahmad, M. and Sun, H. (2017). Three-dimensional ZnO hierarchical nanostructures: solution phase synthesis and applications. *Materials*, 10(11): 1-23.
123. Kołodziejczak-radzimska, A., Markiewicz, E. and Jesionowski, T. (2012). Structural characterisation of ZnO particles obtained by the emulsion precipitation method. *Journal of Nanomaterials,* 2012: 656353.
124. Kurian, M. and Nair, D. S. (2013). Effect of preparation conditions on nickel zinc ferrite nanoparticles : a comparison between sol – gel auto combustion and co-precipitation methods. *Journal of Saudi Chemical Society*, 20(1): 557-522.
125. Sepulveda-guzman, S., Reeja-jayan, B., Rosa, E. De and Torres-castro, A. (2009). Synthesis of assembled ZnO structures by precipitation method in aqueous media. *Materials Chemistry and Physics,* 115: 172-178.
126. Bhosale, M. A., Chenna, D. R. and Bhanage, B. M. (2017). Ultrasound assisted synthesis of gold nanoparticles as an efficient catalyst for reduction of various nitro compounds. *ChemistrySelect,* 2(3): 1225-1231.
127. Deshmukh, A. R., Gupta, A. and Kim, B. S. (2019). Ultrasound assisted green synthesis of silver and iron oxide nanoparticles using fenugreek seed extract and their enhanced antibacterial and antioxidant activities. *Biomed Research International,* 2019: 1714358.
128. Cravotto, G. and Cintas, P. (2006). Power ultrasound in organic synthesis : moving cavitational chemistry from academia to innovative and large-scale applications. *Chemical Society Review,* 2:180-196.
129. Naeimi, H. and Farahnak, M. (2018). A facile one-pot ultrasound-assisted green synthesis of tetrahydrobenzo[b]pyrans catalyzed by gold nanoparticles supported on thiol - functionalized reduced graphene oxide. *Research on Chemical Intermediates*, 44(5): 3227-3247.
130. Hussain, M. (2014). Synthesis, characterization and applications of metal oxide. Dissertation Linköping University.
131. Khaldakar, M. and Butala, D. (2017). The synthesis and characterization of metal oxide nanoparticles and its application for photo catalysis. *International Journal of Scientific and Research Publications*, *7*(3): 499.
132. Tushar G, R. and Babita R, A. (2019). Transmission electron microscopy- an overview. *International Research Journal for Inventions in Pharmaceutical Sciences*, 1(2): 1-7.
133. Inkson, B. J. (2016). Scanning electron microscopy (SEM) and Transmission electron microscopy (TEM) for materials characterization. In *Materials Characterization Using Nondestructive Evaluation (NDE) Methods*. Elsevier Ltd.
134. Mahjoub, A. R., Movahedi, M., Kowsari, E. and Yavari, I. (2014). Narcis-like zinc oxide: Chiral ionic liquid assisted synthesis, photoluminescence and photocatalytic activity. *Materials Science in Semiconductor Processing*, 22(1): 1-6.
135. Kowsari, E. and Karimzadeh, A. H. (2012). Fabrication of fern-like, fish skeleton-like, and butterfly-like BaO nanostructures as nanofillers for radar-absorbing nanocomposites. *Materials Letters*, 74: 33-36.
136. Mourdikoudis, S., Pallares, R. M. and Thanh, N. T. K. (2018). Characterization techniques for

nanoparticles: Comparison and complementarity upon studying nanoparticle properties. *Nanoscale*, 10(27): 12871-12934.

137. Tzani, A., Koutsoukos, S., Koukouzelis, D. and Detsi, A. (2017). Synthesis and characterization of silver nanoparticles using biodegradable protic ionic liquids. *Journal of Molecular Liquids*, 243: 212-218.
138. Nithya, P., Balaji, M., Jegatheeswaran, S., Selvam, S. and Sundrarajan, M. (2017). Facile biological synthetic strategy to morphologically aligned CeO_2/ZrO_2 core nanoparticles using *Justicia adhatoda* extract and ionic liquid: Enhancement of its bio-medical properties. *Journal of Photochemistry & Photobiology, B: Biology*, 2017:1-34.
139. Padovini, D. S. S., Pontes, D. S. L., Dalmaschio, C. J., Pontes, F. M. and Longo, E. (2014). Facile synthesis and characterization of ZrO_2 nanoparticles prepared by the AOP/hydrothermal route. *RSC Advances*, 4(73): 38484-38490.
140. Lu, X., Tao, L., Song, D., Li, Y. and Gao, F. (2018). Bimetallic Pd @ Au nanorods based ultrasensitive acetylcholinesterase biosensor for determination of organophosphate pesticides. *Sensors & Actuators: B. Chemical*, 255: 2575-2581.
141. Shyamala, S., Kalaiarasi, S., Karpagavinayagam, P., Vedhi, C., Muthuchudarkodi, R. R., Kulandaivel, S., and Lakshmi, A. (2021). Synthesis of metal oxide nanoparticles doped poly 3 anisidine nanocomposites with enhanced electrocatalytic activity for methanol oxidation. *Materials Today: Proceedings*, 2021: 3-10.
142. Rakhimol, K. R., Thomas, S., Kalarikkal, N. and Jayachandran, K. (2020). Casein mediated synthesis of stabilized metal/metal-oxide nanoparticles with varied surface morphology through pH alteration. *Materials Chemistry and Physics*, 246: 122803.
143. Itoh, H., Naka, K. and Chujo, Y. (2004). Synthesis of gold nanoparticles modified with ionic liquid based on the imidazolium cation. *Journal of American Chemical Society,* 26(1): 3026-3027.
144. Kowsari, E. and Bazri, B. (2014). Synthesis of rose-like ZnO hierarchical nanostructures in the presence of ionic liquid/Mg2+ for air purification and their shape-dependent photodegradation of SO_2, NOx, and CO. *Applied Catalysis A: General*, 475: 325-334.
145. Husanu, E., Cappello, V., Pomelli, C. S., David, J., Gemmi, M. and Chiappe, C. (2017). Chiral ionic liquid assisted synthesis of some metal oxides. *RSC Advances*, 7(2): 1154-1160.
146. Pulskamp, K., Diabaté, S. and Krug, H. F. (2007). Carbon nanotubes show no sign of acute toxicity but induce intracellular reactive oxygen species in dependence on contaminants. *Toxicology Letters*, 168(1): 58-74.
147. Liu, H., Wang, M., Wang, Y., Liang, Y., Cao, W. and Su, Y. (2011). Ionic liquid-templated synthesis of mesoporous CeO2-TiO 2 nanoparticles and their enhanced photocatalytic activities under UV or visible light. *Journal of Photochemistry and Photobiology A: Chemistry*, 223(2-3): 157-164.
148. Ismail, A. A., van de Voort, F. R. and Sedman, J. (1997). Chapter 4 Fourier transform infrared spectroscopy: Principles and applications. *Techniques and Instrumentation in Analytical Chemistry*, 18(C): 93-139.
149. Bodade, A. B., Taiwade, M. A. and Chaudhari, G. N. (2017). Bioelectrode based chitosan-nano copper oxide for application to. *Journal of Applied Pharmaceutical Research,* 5: 30-39.
150. Alomairy, S., Al-Buriahi, M. S., Abdel Wahab, E. A., Sriwunkum, C. and Shaaban, K. S. (2021). Synthesis, FTIR, and neutron/charged particle transmission properties of Pb_3O_4–SiO_2–ZnO–WO_3 glass system. *Ceramics International*, 47(12): 17322-17330.
151. Kumar, A. (2020). Sol gel synthesis of zinc oxide nanoparticles and their application as nano-composite electrode material for supercapacitor. *Journal of Molecular Structure*, 1220: 128654.
152. Nithya, P., Balaji, M., Mayakrishnan, A. and Jegatheeswaran, S. (2020). Biogenic approach for the synthesis of Ag-Au doped RuO_2 nanoparticles in BMIM-PF_6 ionic liquid medium: Structural characterization and its biocidal activity against pathogenic bacteria and HeLa cancerous cells. *Journal of Molecular Liquids*, 312: 113245.
153. Goharshadi, E. K., Samiee, S. and Nancarrow, P. (2011). Fabrication of cerium oxide nanoparticles: Characterization and optical properties. *Journal of Colloid and Interface Science*, 356(2): 473-480.
154. Rajesh, G. and Nagar, A. (2018). Efficacy of calcination on the optical, structural and photocatalytic properties of Zirconium Oxide via facile precipitation method. *Journal of Emerging Technologies and Innovative Research, 5*(10): 575-585.

155. Devanand Venkatasubbu, G., Ramasamy, S., Ramakrishnan, V. and Kumar, J. (2013). Folate targeted PEGylated titanium dioxide nanoparticles as a nanocarrier for targeted paclitaxel drug delivery. *Advanced Powder Technology*, 24(6): 947-954.
156. Ramzan, M., Obodo, R. M., Mukhtar, S., Ilyas, S. Z., Aziz, F. and Thovhogi, N. (2019). Green synthesis of copper oxide nanoparticles using Cedrus deodara aqueous extract for antibacterial activity. *Materials Today: Proceedings*, 36: 576-581.
157. Garg, S., Gautam, S., Pal, J., Kandasami, A. and Goyal, N. (2021). Materials Characterization Characterizing the defects and ferromagnetism in metal oxides : The case of magnesium oxide. *Materials Characterization*, 179(5): 111366.
158. Nair, H., Liszka, M. J., Gatt, J. E. and Baertsch, C. D. (2008). Effects of metal oxide domain size, dispersion, and interaction in mixed WOx / MoOx catalysts supported on Al_2O_3 for the partial oxidation of ethanol to acetaldehyde. *Journal Physical Chemistry,* 112: 1612-1620.
159. Bharate, B. G., Hande, P. E., Samui, A. B. and Kulkarni, P. S. (2018). Ionic liquid (IL) capped MnO_2 nanoparticles as an electrode material and IL as electrolyte for supercapacitor application. *Renewable Energy*, 126: 437-444.
160. Bunaciu, A. A., Udriştioiu, E. gabriela, and Aboul-Enein, H. Y. (2015). X-ray diffraction: Instrumentation and applications. *Critical Reviews in Analytical Chemistry*, 45(4): 289-299.
161. Connolly, J. R. (2005). Introduction to X-ray powder diffraction. *Spring*, 2005: 1-9.
162. Zangaro, G. A. C., Carvalho, A. C. S., Ekawa, B., do Nascimento, A. L. C. S., Nunes, W. D. G., Fernandes, R. P., Parkes, G. M. B., Ashton, G. P., Ionashiro, M. and Caires, F. J. (2019). Study of the thermal behavior in oxidative and pyrolysis conditions of some transition metals complexes with Lornoxicam as ligand using the techniques: TG-DSC, DSC, HSM and EGA (TG-FTIR and HSM-MS). *Thermochimica Acta*, 681(8): 178399.
163. Amaya, S. L., Alonso-Núñez, G., Díaz De León, J. N., Fuentes, S. and Echavarría, A. (2021). Synthesis and characterization of metal oxides complexes with potential application in HDS reactions. *Materials Letters*, 291: 129562.
164. Kowsari, E. and Abdpour, S. (2016). Investigation performance of rod-like ZnO/CdO composites, synthesized in ionic liquid medium as photocatalytic for degradation of air pollutants (SO_2 and NO_X). *Optik*, 127(23): 11567-11576.
165. Singh, N. and Haque, F. Z. (2016). Synthesis of zinc oxide nanoparticles with different pH by aqueous solution growth technique. *Optik*, 127(1): 174-177.
166. Kowsari, E. and Abdpour, S. (2017). In-situ functionalization of mesoporous hexagonal ZnO synthesized in task specific ionic liquid as a photocatalyst for elimination of SO2, NOx, and CO. *Journal of Solid State Chemistry*, 256(9): 141-150.
167. Salleh, A., Naomi, R., Utami, N. D., Mohammad, A. W., Mahmoudi, E., Mustafa, N. and Fauzi, M. B. (2020). The potential of silver nanoparticles for antiviral and antibacterial applications: A mechanism of action. *Nanomaterials*, 10(8): 1-20.
168. Issn, O. P. and Sarkar, S. (2020). Silver nanoparticles with bronchodilators through nebulisation to treat Covid-19 patients. *Journal of Current Medical Researcg and Opinion*, 3(4): 449-450.
169. Shereen, M. A., Khan, S., Kazmi, A., Bashir, N. and Siddique, R. (2020). Covid-19 Infection: Origin, transmission, and characteristics of human coronaviruses. *Journal of Advanced Research*, 24: 91-98.
170. El-Shishtawy, R. M., Asiri, A. M., Abdelwahed, N. A. M. and Al-Otaibi, M. M. (2011). In situ production of silver nanoparticle on cotton fabric and its antimicrobial evaluation. *Cellulose*, 18(1): 75-82.
171. Jia, M., Zhang, W., He, T., Shu, M., Deng, J., Wang, J., Li, W., Bai, J., Lin, Q., Luo, F., Zhou, W. and Zeng, X. (2020). Evaluation of the genotoxic and oxidative damage potential of silver nanoparticles in human NCM460 and HCT116 cells. *International Journal of Molecular Sciences*, 21(5): 1618.